National Library of Canada
Acquisitions and Bibliographic Services Branch
395 Wellington Street
Ottawa, Ontario
K1A 0N4

Bibliothèque nationale du Canada
Direction des acquisitions et des services bibliographiques
395, rue Wellington
Ottawa (Ontario)
K1A 0N4

Your file Votre référence

Our file Notre référence

NOTICE

The quality of this microform is heavily dependent upon the quality of the original thesis submitted for microfilming. Every effort has been made to ensure the highest quality of reproduction possible.

If pages are missing, contact the university which granted the degree.

Some pages may have indistinct print especially if the original pages were typed with a poor typewriter ribbon or if the university sent us an inferior photocopy.

AVIS

La qualité de cette microforme dépend grandement de la qualité de la thèse soumise au microfilmage. Nous avons tout fait pour assurer une qualité supérieure de reproduction.

S'il manque des pages, veuillez communiquer avec l'université qui a conféré le grade.

La qualité d'impression de certaines pages peut laisser à désirer, surtout si les pages originales ont été dactylographiées à l'aide d'un ruban usé ou si l'université nous a fait parvenir une photocopie de qualité inférieure.

Canada

Studies of Turbulence with a Wind Profiler

Sylvain G. Leblanc

Department of Atmospheric And Oceanic Sciences
McGill University, Montreal

August 1994

A thesis submitted to the Faculty of
Graduate Studies and Research
in partial fulfillment of the requirements
of degree of Master of Science

ISBN 0-612-05578-7

Canada

à la personne la plus patiente et généreuse sur terre:

ma mère

Abstract

In Doppler radar analysis of the atmosphere the spectrum width is rarely used but it contains information about turbulence. Turbulence is not the only effect that contributes to the broadening of the spectrum. Another effect is the cross-beam wind, which can be dominant in broad-beam radars such as wind profilers. Once this effect is removed, the so-called residual width then serves as an indication of turbulence. A large snowstorm is used in this study for the computation of the residual width. Strong wind and wind shear were observed during the storm. The time-height pattern of residual width bears a close resemblance to that of wind shear. This supports the interpretation of the residual width as being an indication of turbulence induced by wind shear. Energy dissipation rates are also estimated for the snowstorm. In some regions values as large as 800 cm^2s^{-3} are observed. These are large, but within the range of what has been reported by others. The same techniques were applied to the study of clear-air turbulence to relate radar reflectivity with turbulence.

Résumé

Dans l'étude de l'atmosphère à l'aide d'un radar Doppler, la largeur du spectre est rarement utilisée, mais elle contient de l'information sur la turbulence. La turbulence n'est pas le seul effet qui contribue à l'augmentation de la largeur du spectre. Une autre cause de cette augmentation est le vent horizontal qui coupe le faisceau, cet effect est dominant pour les radars avec un faisceau large comme les profilateurs de vents. Une fois cet effet enlevé, la largeur résiduelle du spectre sert d'indice de turbulence. Pour ce mémoire une tempète de neige très intense est la source de données pour le calcul de la largeur résiduelle. Durant cette tempète les vents ainsi que le scisaillement du vent étaient très important. Le patron, en coordonné temps-hauteur, de la largeur résiduelle du spectre ressemble de près a celui du scisaillement de total du vent. Ceci supporte l'interprétation de la largeur résiduelle comme étant un indice de turbulence induit par un scisaillement de vent. Des estimations du taux de changement de dissipation de l' énergie sont présentées. Dans certaines regions des valeurs de 800 cm^2s^{-3} ont été observées. Ce sont de grandes valeurs, mais elles sont dans les limites des mesures fait par d'autres dans le passé. Ensuite les techniques utilisées pour la neige sont appliquées à l' étude de l'air clair pour relier la reflectivité des radars à la turbulence.

Acknowledgements

I would like to acknowledge everyone who helped and advised me on this thesis: Steve Cohn, Fiona Drummond, Frédéric Fabry, Zonghui Huo, Phoebe Lam, Karl McGillevray, François Turcotte, Paul Vaillancourt, and especially my supervisor Prof. R.R. Rogers.

Contents

List of Figures

Chapter 1

Introduction

Measurement of turbulence with radar is not a new topic. One of the first estimates of turbulence in a snow event using a Doppler radar was made by Rogers and Tripp [19] in 1964. They concluded that the rms turbulent wind in snow ranges from 0.4 to 2 m/s and that the turbulence of a scale smaller than the radar resolution (in their case about 100 m) contains 75 % of the eddy energy, the rest being in larger scales. Atlas and Srivastava [1] described a method to measure turbulence with a non-Doppler radar and made comparisons with a method used with a Doppler radar, a method similar to the one used in chapter 3 of this thesis. Børresen [3] in 1971 did a study of turbulence and wind shear in a snowstorm, using the Doppler spectral variance. He concluded that the turbulent areas correspond in general to a zone where the total vectorial shear measured over a 600 m interval exceeded 10^{-2}sec^{-1}. More recently in 1990, Sato [21] also used the spectral width to find regions of turbulence with a vertically pointing radar. Hardy and Gage [11] reviewed the history of radar studies of clear air, and Gossard [8] reviewed the radar research on the atmospheric boundary layer, in which he includes turbulence. Hocking [13, 15] also reported measurements of turbulence. His measurements were made not in precipitation but in clear air. He used the spectral widths to calculate energy dissipation rates from clear-air echoes.

The main objective of the research in this thesis is to measure turbulence with a different kind of radar, a small wind profiler. The first goal is to derive the field of turbulence associated with a snowstorm by examining the width of the Doppler spectrum of the vertical velocity, removing the contamination of the cross-beam wind component. The relation between this field and the wind shear is analysed. An analysis of turbulence in scales larger than the radar volume is also included, based on a study of the time variations of the mean vertical Doppler velocity. Estimation of the energy dissipation rate is made using methods developed by Frisch & Clifford [7] and Hocking [13]. The spectral width and the radar reflectivity are used to investigate echoes which result from refractive index fluctuations in the clear atmosphere.

Chapter 2 is a description of the equipment, mainly the wind profiler, used in this research. In Chapter 3 the theory for retrieval of turbulence from the spectral width is explained as well as the different aspects of turbulence as seen by a wind profiler. Chapter 4 contains the data and analysis of the March 13, 1993 snowstorm. It contains information from the wind profiler pertinent to the study of turbulence. Chapter 5 is an attempt to estimate the field of energy dissipation rate for the snowstorm. Chapter 6 deals with interpretation of clear-air turbulence using the spectral width and the radar reflectivity. Different examples of clear-air echoes are analysed in that chapter.

Chapter 2

Equipment

Since May 1992, the Department of Atmospheric and Oceanic Sciences of McGill University has operated a small, UHF wind profiler on the roof of its building in downtown Montreal. It is one of a series of boundary-layer profilers designed by the NOAA Aeronomy Laboratory. It is a 5-beam system, employing a vertical beam and four oblique beams at 21° from the zenith in the North, South, East and West directions. It uses a wavelength of 32.8 cm and has about the same sensitivity to moderately reflecting clear air as to light rain. For the observations used in this study, the range resolution was 105 m. Table 1 contains all the relevant parameters.

A wind profiler needs at least two orthogonal oblique beams and a vertical beam to compute the wind accurately. The two extra beams in our system are not standard for a wind profiler; they can give a better accuracy of the measurements, but usually only research profilers have five beams. The beams work in sequence. The sequence used in this research was one vertical beam then the four other beams: Vertical-East-North-South-West.

The recorded data consist of complete Doppler spectra at typically 50 positions in range. Collecting data for one beam takes approximatly 30 s. A complete cycle then takes around 2.5 minutes. This can give us information for up to 24 individual wind profiles per hour. With those different profiles we usually do a consensus

average over 15 or 30 min. This then gives two or four average wind profiles per hour. When no precipitation is present, the profiler can often detect clear-air echoes and measure the wind up to an altitude of about 3 km. Usually during stratiform precipitation, the radar detects echoes up to 5 km. In showers and thunderstorms the range can extend to 10 km.

Table 1. Montreal Wind Profiler characteristics used during the Storm of the Century

Frequency	915 MHz
Wavelength	32.8 cm
Peak Power	500 W
Antenna Aperture	1.8 m x 1.8 m
Antenna Type	64 element array
Number of Beams	5
Pointing Directions	Vertical; 21° zenith angle at cardinal points
Beamwidth	9°
Pulse duration	0.7 μ s
Interpulse Period	49-56 μ s
Range resolution	105 m
Number of Range Samples	30-80
Maximum Radial Velocity	$\pm$ 10-23.7 m/s
Number of Spectral Points	64

The data collected are written to an optical disk. Once the disk is full the data can be used for analysis. The data are transfered to a Silicon Graphics workstation from which we do the analysis. Regular plots made for the archives include consensus winds and summary plots of reflectivity and mean Doppler velocity in the vertical beam. The profiler operates continuously. Since October 1993, a Radio Acoustic Sounding System (RASS) has been added to the profiler to measure the hourly temperature profiles up to a varying altitude which is ordinarily about 800 m.

Chapter 3

Theoretical background

3.1 Radar velocity spectrum

A Doppler radar measures the position and the radial velocity of a target. The convention for the Montreal Wind Profiler (MWP) is that positive velocities are towards the radar and negative, away. This is done by measuring the difference between the frequency transmitted and the frequency returned to the radar. Frequency is related to radial velocity by

$$\Delta f = \frac{2v_r}{\lambda}, \tag{3.1}$$

where λ is the wavelength of the radar and Δf is the change in frequency between the emission and the reception of the signal, the Doppler shift. The radial velocity, positive towards the radar, is related to the velocity vector $\mathbf{V}$ of the scatterer by $v_r = -\mathbf{V} \cdot \mathbf{r}$ where r is a unit vector in the radar pointing direction. The region where the radar measures data is the pulse volume. The number of scatterers found in that volume is usually very large so that the distribution of their velocities can be approximated by a continous distribution. This distribution is called the Doppler spectrum s(v) and usually approximates a Gaussian shape. Fig. 3.1 shows a real spectrum of velocity. It can be described by its width or variance ; spectral variance σ_s^2 and its mean velocity :$< v_r >$. They are the first and second moments of the

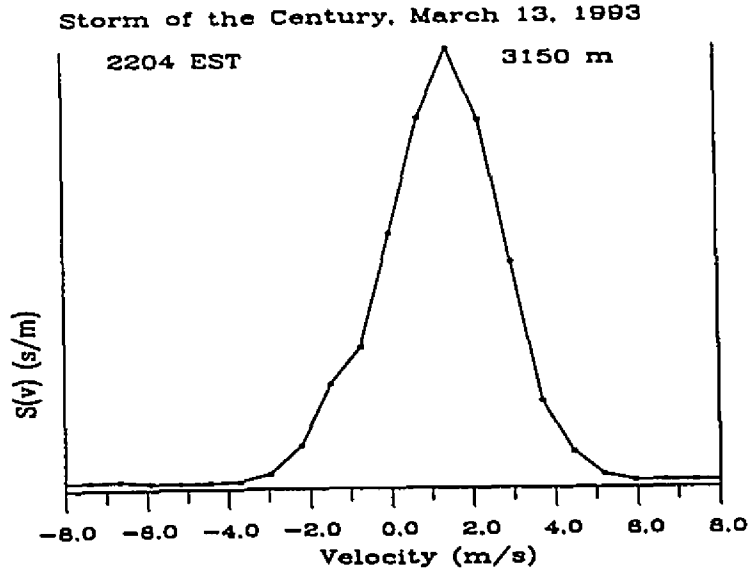

Figure 3.1: Doppler Spectrum of snow in vertical beam

spectrum. In general the mean velocity is the quantity used for physical interpretation such as the computation of the wind field. By using both the mean velocity of the spectrum and the width, and their variation with time, we can have information about the turbulence in the atmosphere. The present research deals with the data taken from the vertical beam only; the other beams serve for the computation of the wind consensus.

3.2 Turbulence

Atmospheric turbulence exists over a range of scales. The wind profiler is affected by those scales in different ways. The scales generally smaller than the sampled volume contribute to the spectral width; those larger than the volume show up as time variations in the mean Doppler velocity (Rogers and Tripp [18]). Figure 3.2 illustrates the effect schematically. Small-scale irregularities in the wind introduce a range of Doppler velocities in any measurement, but have little effect on the mean. Large-scale irregularities, on the other hand, shift the entire spectrum one way or

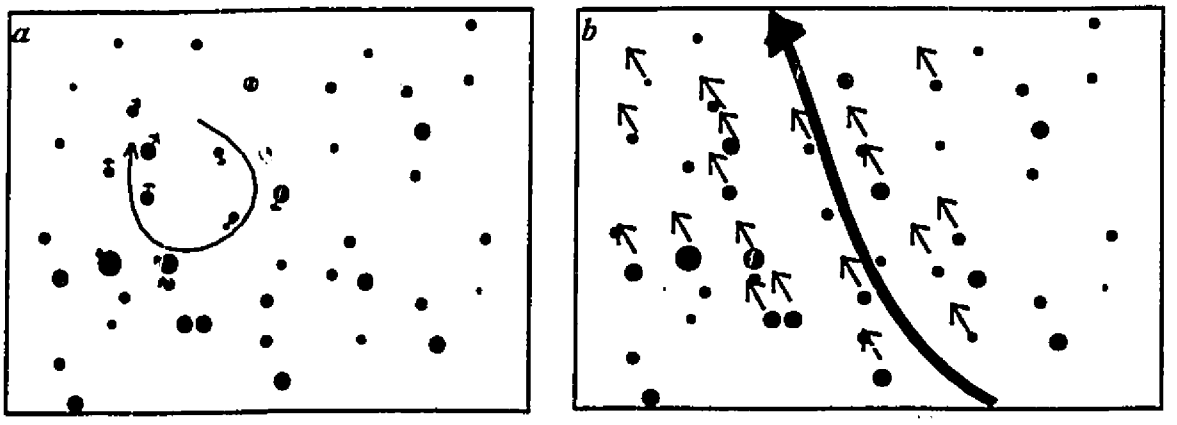

Figure 3.2: Pulse volume a) Small scale turbulence, b) large scale

the other without strongly affecting the spectral width. In fact the variance of the mean vertical velocity $\sigma^2_{<v>}$ over a certain period of time gives us information about the energy content of the large scale turbulence .

The problem is that turbulence is not the only factor that causes a broadening of the spectrum. The important factors for a vertical beam are [21]:

- the horizontal wind blowing the scatterers across the beam
- different fall speeds of the scatterers
- small scale turbulence

Assuming independence of each factor the variance of the Doppler spectrum σ_s^2 is then the summation of all the different broadening variances[21]:

$$\sigma_s^2 = \sum_i \sigma_i^2 = \sigma_t^2 + \sigma_f^2 + \sigma_w^2, \tag{3.2}$$

where σ_t^2 is the variance from the small scale turbulence, σ_f^2 is the variance due to the fall speed distribution of the scatterers and σ_w^2 is the variance due to the cross-beam wind. If we subtract the last two processes from σ_s^2 , we can then determine the variance due to small scale turbulence. An estimate of the total velocity variance due

to turbulence over a certain averaging time is then obtained by adding the average variance to the variance of the mean Doppler velocity [19]; $\sigma^2_{T_{ot}} = < \sigma^2_t > + \sigma^2_{<v>}$

3.3 Broadening of the spectrum by the horizontal wind

Because of the finite width of the beam, horizontal winds that cross the vertical beam affect the information received by that beam. If we look at Fig. 3.3 , at point *a* the profiler sees a vertical velocity larger then the real value because the horizontal wind has a component in the direction of the profiler. But at point *b* the component is opposite to the profiler. The effect can be approximated for a vertically pointing beam as [12]

$$\sigma^2_w = 0.09\theta^2 V^2, \tag{3.3}$$

where V is the speed of the horizontal wind and θ is the beamwidth. Figure 3.4 shows this relation for a 9° beamwidth. This relation has been used in the past by Børresen [3], and Hocking [15], in studies of turbulence. The effect of the horizontal wind is the most important broadening factor in many of our observations, and it is removed from the Doppler variance in this research to give us information about turbulence.

3.4 Broadening of the spectrum by differential fall speed

When dealing with precipitation, the fall speed distribution also contributes to the broadening of the spectrum. Snow usually falls between 1-2 m/s. Hitschfeld and Dennis [12] have calculated that this gives a Doppler standard deviation of 0.25 m/s at most. Using some simple assumptions, it can be proven that this contribution is

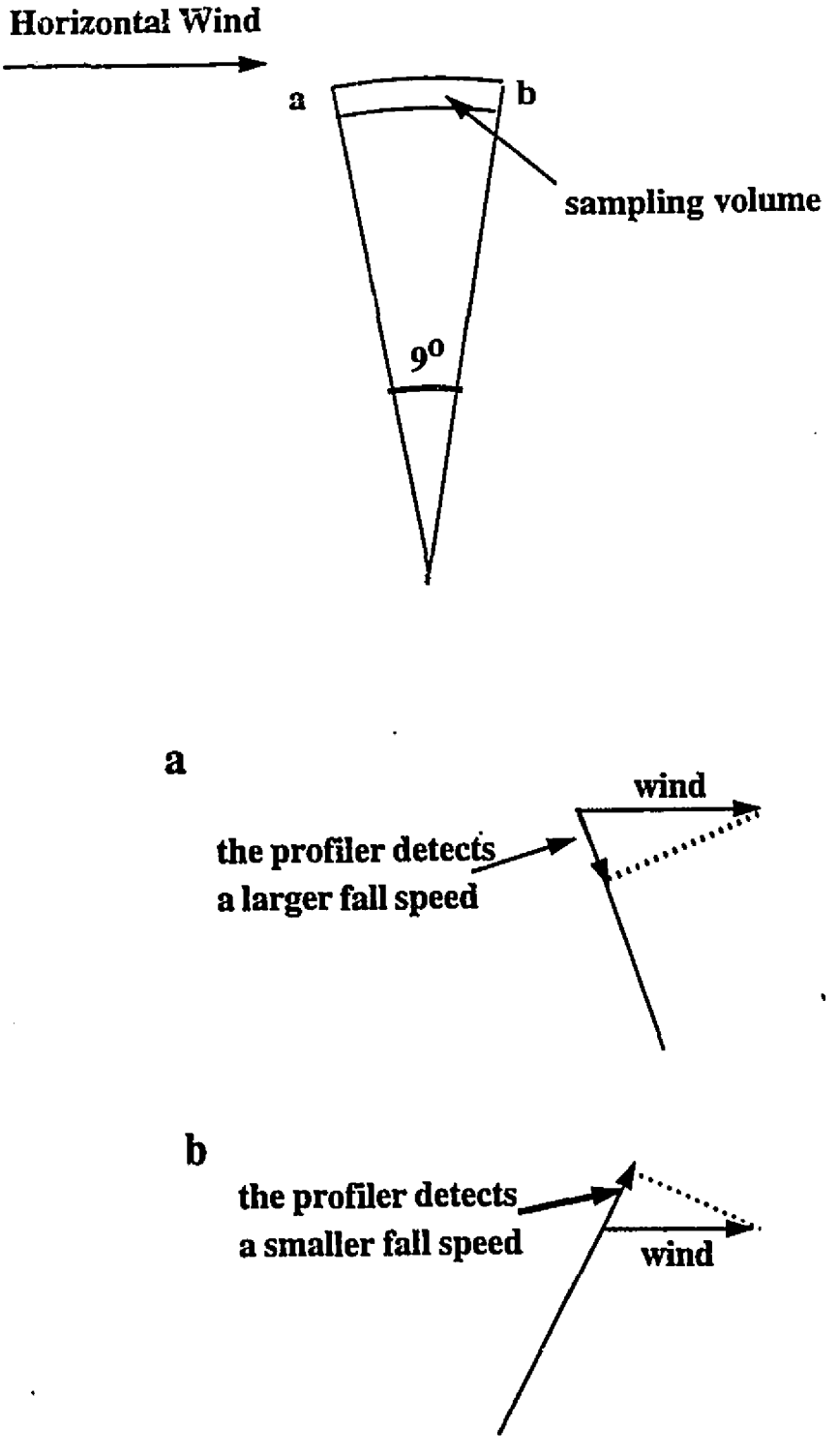

Figure 3.3: Broadening of the Spectrum by the Horizontal Wind

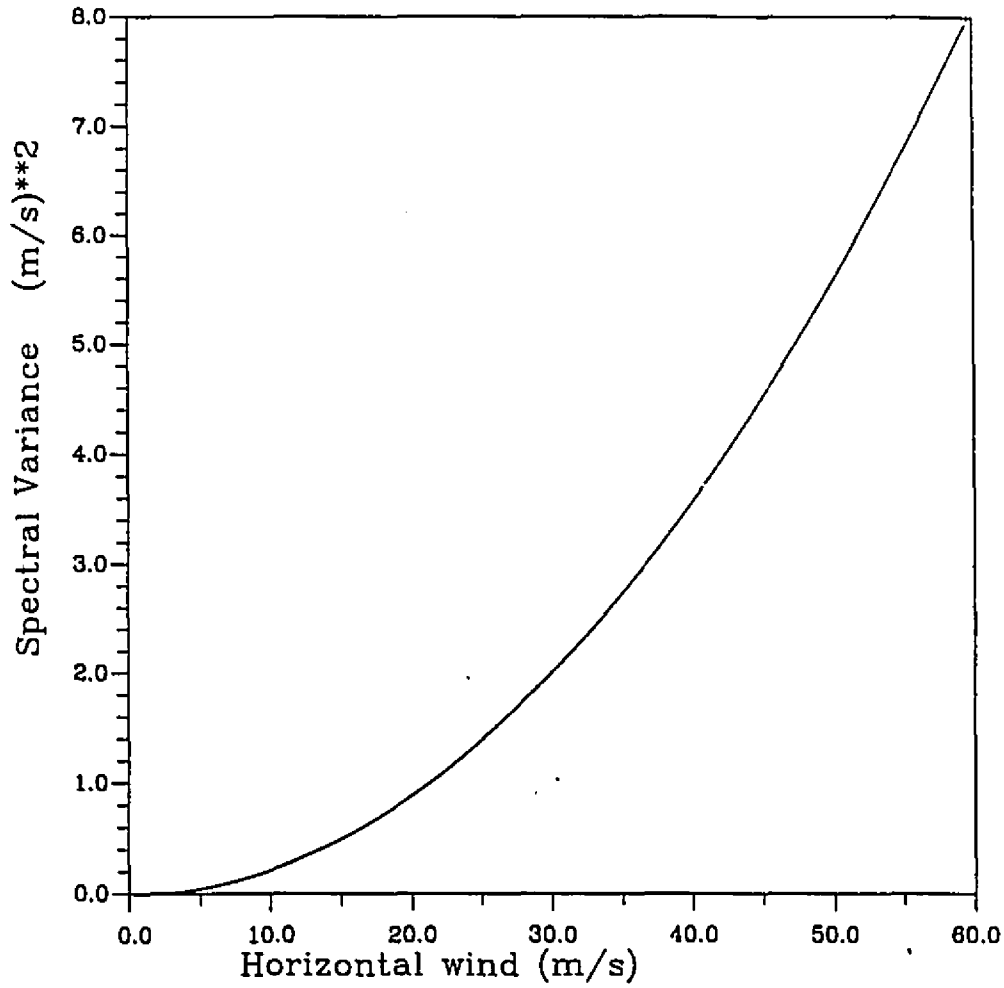

Figure 3.4: Spectral Variance vs Horizontal Wind Speed for the 9° Beam of the Montreal Wind Profiler

negligible in normal situations . The first assumption is a general one. We assume an exponential size distribution of snowflakes in the form of

$$N(D) = N_o e^{-\Lambda D} \tag{3.4}$$

with

$$N_o(cm^{-4}) = 2.5 \times 10^{-2} R^{-0.94} \tag{3.5}$$

and

$$\Lambda(cm^{-1}) = 22.9 R^{-0.45}, \tag{3.6}$$

where D is the melted diameter and R the precipitation rate in mm/h [20]. The reflectivity Z, can be found with

$$Z = \int_0^\infty N(D) D^6 dD, \tag{3.7}$$

it gives

$$Z = \frac{N_o 6!}{\Lambda^7}. \tag{3.8}$$

Now using approximate relations for snow from Langleben [17], the fall speeds at the ground have the form of

$$v_s = AD^B, \tag{3.9}$$

where A and B depend on the kind of snowflake, and D is the melted diameter in cm. Typical values of the parameters are 160 and 234 for A and 0.3 for B, depending on the kind of snowflake (dendrite or columns and plates). Now we need to calculate the mean fall speed and the mean of the fall speed squared (both reflectivity weighted) to find the variance of the Doppler spectrum. The mean speed is

$$< v_s >= \frac{1}{Z} \int_0^\infty v_s N(D) D^6 dD. \tag{3.10}$$

Replacing v_s from Eq. 3.9 we obtain

$$< v_s >= \frac{A}{Z} \int_0^\infty N(D) D^{6+B} dD. \tag{3.11}$$

Integrating Eq. 3.11 gives

$$< v_s >= \frac{AN_o}{Z} \frac{\Gamma(7+B)}{\Lambda^{7+B}}. \tag{3.12}$$

By replacing Λ from Eq. 3.8 we find

$$< v_s >= \frac{AN_o\Gamma(7+B)}{Z} \left(\frac{Z}{6!N_o}\right)^{(7+B)/7}, \tag{3.13}$$

which gives as value for dendrites in cgs;

$$< v_s >= 213 \left(\frac{Z}{N_o}\right)^{0.043}. \tag{3.14}$$

In conventional units

$$< v_s >= 0.65 \left(\frac{Z}{N_o}\right)^{0.043}, \tag{3.15}$$

where $< v_s >$ is in m/s and Z in $\mathrm{mm^6 m^{-3}}$. Similarly the mean square fall speed is

$$< v_s^2 >= \frac{A^2N_o\Gamma(7+2B)}{Z} \left(\frac{Z}{6!N_o}\right)^{(7+2B)/7}. \tag{3.16}$$

With A = 160 and B = 0.3 we find

$$< v_s^2 >= 46024 \left(\frac{Z}{N_o}\right)^{0.086}, \tag{3.17}$$

again in the proper units($< v_s^2 >$ in m^2s^{-2} and Z in mm^6m^{-3}) ;

$$< v_s^2 >= 0.43 \left(\frac{Z}{N_o}\right)^{0.086}. \tag{3.18}$$

The variance is

$$\sigma_f^2 =< v_s^2 > - < v_s >^2 = 6.0 \times 10^{-3} \left(\frac{Z}{N_o}\right)^{0.086}. \tag{3.19}$$

Assuming a typical Z-R relation for snow in the form of [10]

$$Z = 2000R^2 \tag{3.20}$$

and using this relation with Eq: 3.5 gives

$$N_o = 0.89 Z^{-0.47}. \tag{3.21}$$

Inserting Eq 3.21 in Eq:3.19 leads to

$$\sigma_f^2 = 6.1 \times 10^{-3} Z^{0.13}, \tag{3.22}$$

where Z is in mm^6m^{-3} and σ_f^2 in m^2s^{-2}. The reflectivity in the snow never exceeds 50 dBZ. This high reflectivity would give $\sigma_f^2 = 0.03$ m^2s^{-2}, which is often negligible compared to the values observed. For columns and plates ; A = 234 and B = 0.3, so

$$\sigma_f^2 = 1.3 \times 10^{-2} Z^{0.13}, \tag{3.23}$$

with Z is in mm^6m^{-3} and σ_f^2 in m^2s^{-2}. For 50 dBZ, this gives $\sigma_f^2 = 0.04$ m^2s^{-2}, a value also negligible compared to most of the observed values of the spectral variance. Since this effect does not broaden the spectrum in a significant way, the turbulence field may be aproximaed by $\sigma_s^2 - \sigma_w^2$.

Chapter 4

Data and Analysis of the Storm of the Century

4.1 Observations

During the weekend of March 13 and 14, 1993, Montreal had one of its biggest snowstorms in years. More than 40 cm of snow reached the ground in less than 24 hours. This storm is commonly called the storm of the century because of its intensity, especially in the United States. The storm was less intense in Montreal. But still this set of data is one of the best examples of a snowstorm the wind profiler has recorded since the beginning of its operation in 1992. The data used in this research are from 1000 EST on March 13 before the snow started to fall on the ground to 1000 EST on March 14 after the snow stopped. That represents nearly 575 beam cycles, which include approximately 34500 spectra for each beam.

To reduce the effects of ground clutter and external radio-frequency interference, the data were filtered based on the signal to noise ratio. All values having SNR less than -5 dB were rejected. Fig 4.1 shows the field of SNR for the entire duration of the storm, 24 hours of data with altitudes ranging from 210 meters above the profiler to almost 8 kilometers. One reason for choosing the -5 dB threshold is

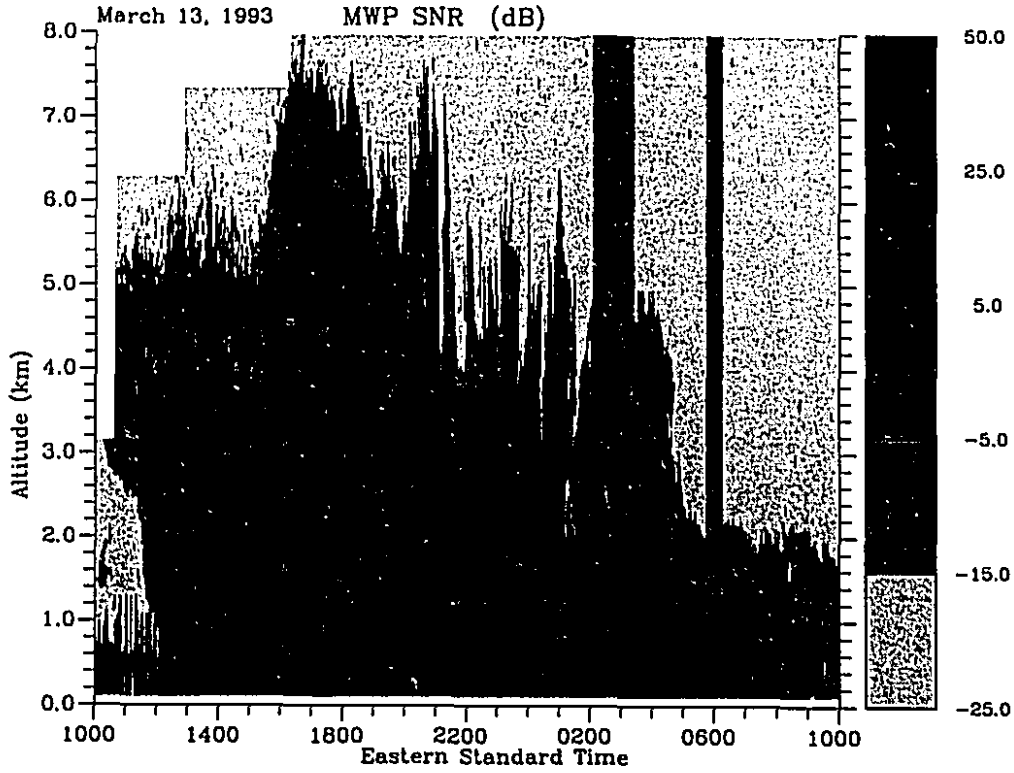

Figure 4.1: Signal To Noise Ratio field

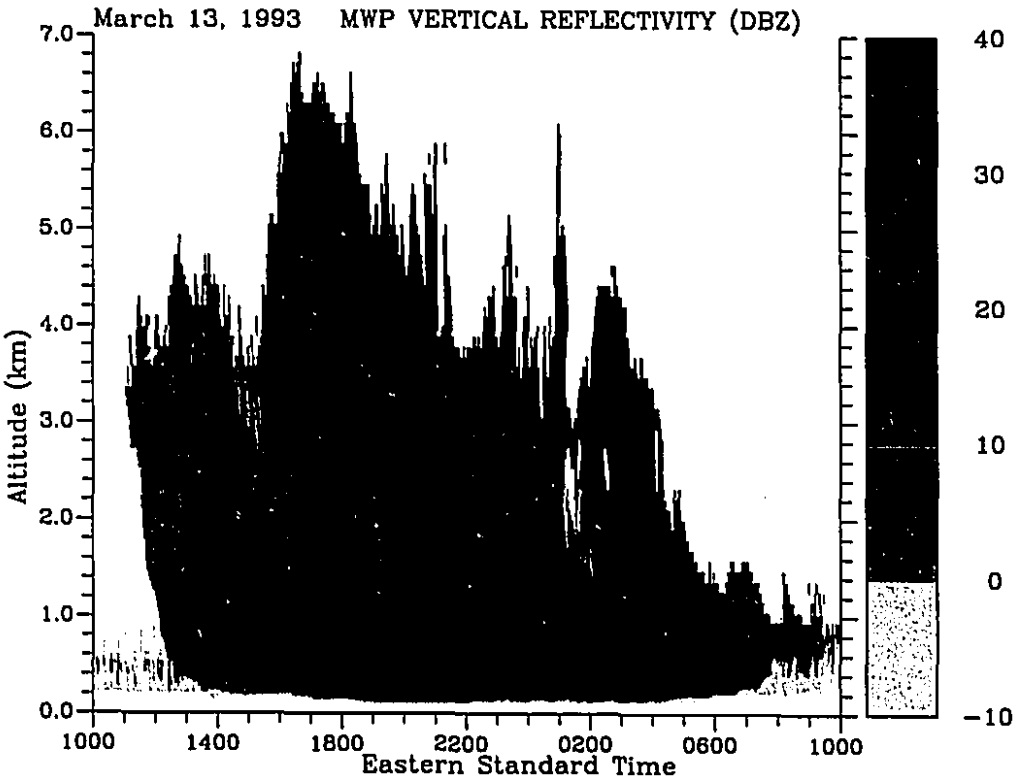

Figure 4.2: Reflectivity field

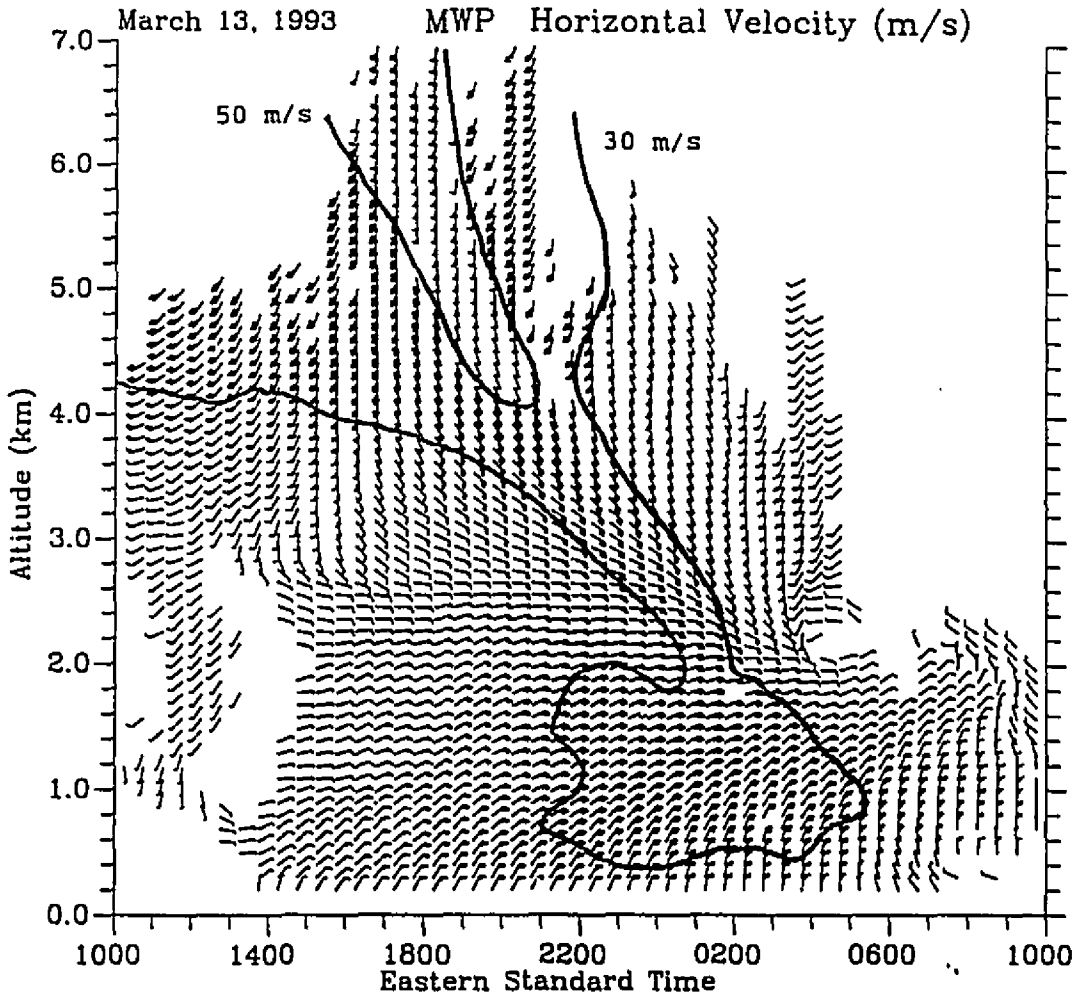

Figure 4.3: Horizontal Wind field

that it removes most of the extraneous interference that occurred between 0300 and 0600 on March 14. The rest of the interference was removed by an algorithm in the programs which analyses the data. For most of the data used the SNR is very high. We had values of more than 20 dB that day during the strong part of the storm when most of the snow was reaching the ground, between 1800 on March 13 and 0400 on March 14. This is clear from the reflectivity field of Fig 4.2.

One thing to note on Fig. 4.1, around 0100 at 2 km in height, is that there is

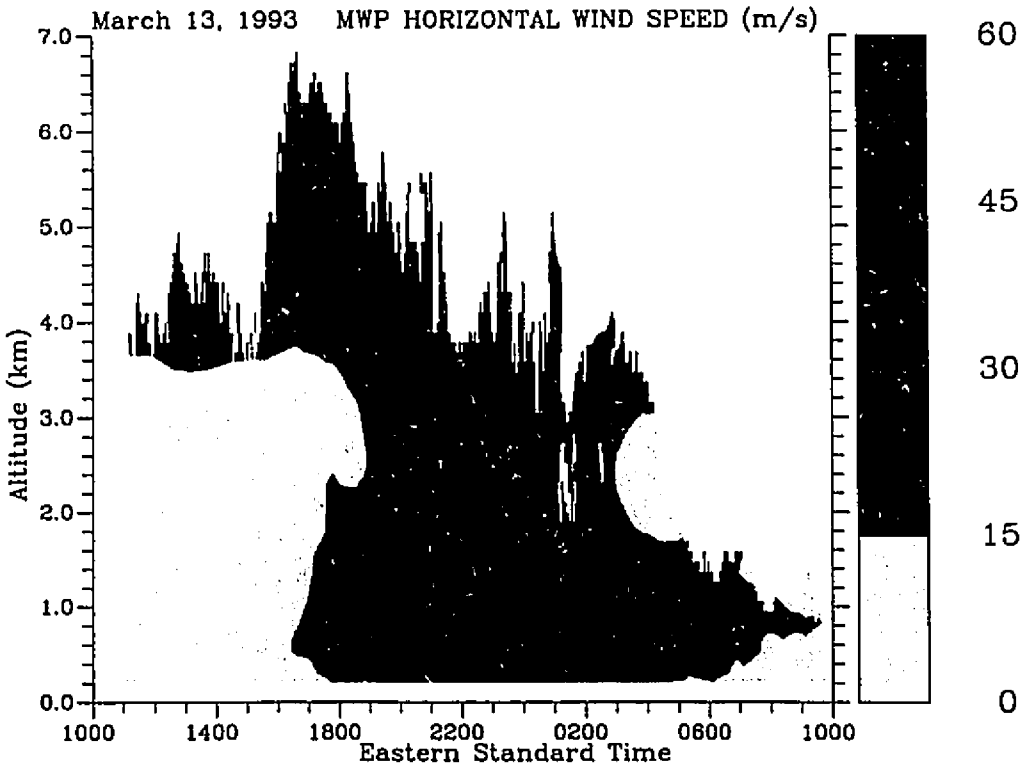

Figure 4.4: Wind Speed field

a region of weaker SNR which gives "holes" in our dataset. The SNR field and the reflectivity are naturaly closely related: a strong reflectivity gives a strong signal.

Fig. 4.3 shows the wind field over Montreal for the duration of the snowstorm. The two contour lines are for winds stronger than 30 m/s and 50 m/s. Regions where winds are not plotted can be due to either low signal to noise ratio or failure to achieve a consensus for the averaging period. Fig. 4.3 has the wind averaged over 30 minutes for the simplicity of the plot but a 15-minute consensus was used in the analysis described later. Figure 4.3 shows that the most important change in the direction is at about midnight on March 13. The winds were light at the beginning of the storm, but became quite intense after 2200 and in fact continued to be strong on the morning of March 14.

To give a better indication of the wind speed, Fig. 4.4 is a plot of the speed with a consensus time of 15 minutes. A low-level jet at about 1 km can be seen on

both Fig. 4.3 and 4.4 between 2200 and 0700.

4.2 Residual Variance

The data taken from the vertical beam give us the vertical velocity of the scatterers with respect to the ground. Figure 4.5 is the mean vertical velocity field for this case. The values are all close to 1 m/s, in fact 75% of the values calculated for the vertical velocity are between 0.5 and 1.5 m/s. We have 28858 data points on this plot. It is clear from the downward velocities that all the precipitation was in the form of snow for that day. At the beginning and the end of the 24-hour period, we can see negative values for the vertical velocity (3.45 % of the total), which would ordinarily mean that the scatterers were moving upwards. Because the observations are at close range and at times with little or no snow to provide an echo, they may be due to ground clutter. Except for these data at low altitudes at the beginning and at the end of the plot, this is a very good set of observations.

In chapter 3 we saw that the spectral variance σ_s^2 is composed of three major parts: σ_t^2 , σ_f^2 and σ_w^2 . If we remove the variance σ_w^2 due to the cross beam wind from the total spectral variance σ_s^2 this should give an approximation of turbulence since the variance due to differential fall speed σ_f^2 is negligible in snow. We call the result of this subtraction σ_r^2, the residual variance. Thus,

$$\sigma_r^2 = \sigma_s^2 - \sigma_w^2. \tag{4.1}$$

Fig. 4.6 is the field of the total spectral variance σ_s^2 for the storm. We can clearly see the increase of the variance in time at all altitudes during the first half of the storm.

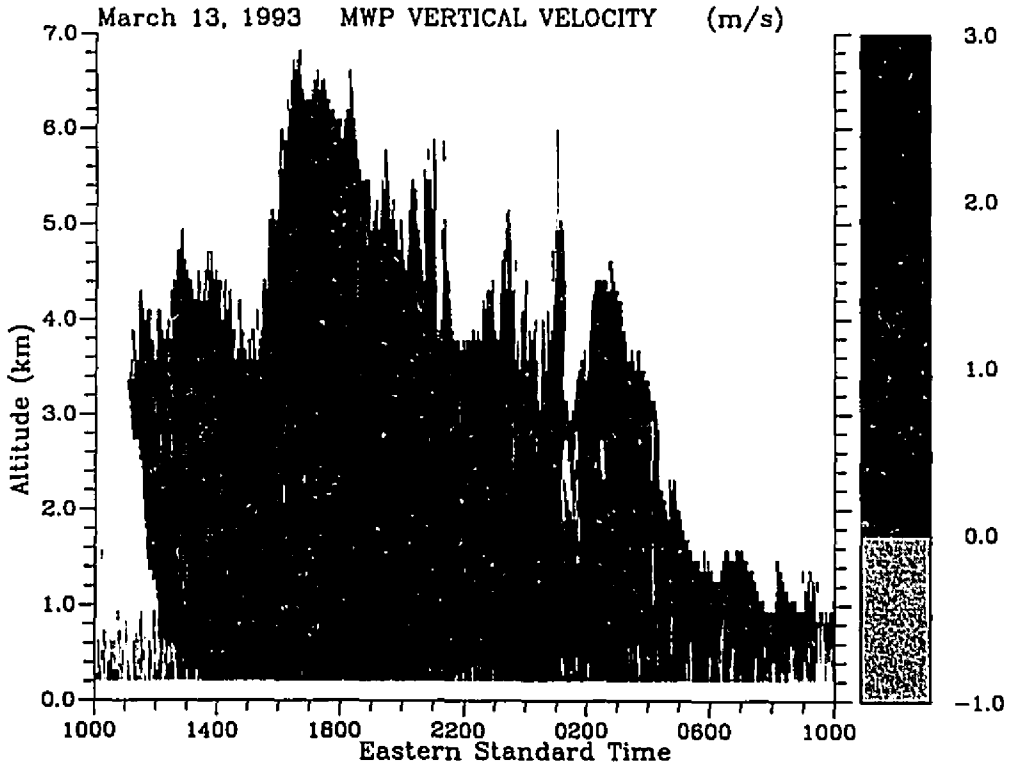

Figure 4.5: Vertical Velocity Field

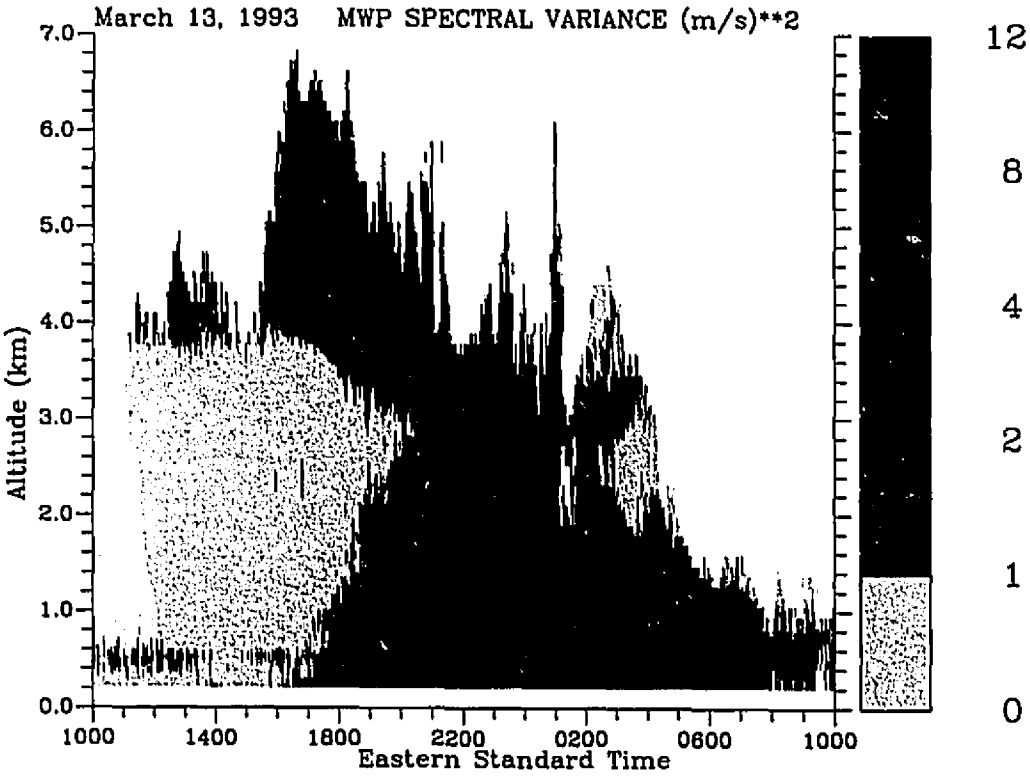

Figure 4.6: Spectral Variance σ_s^2

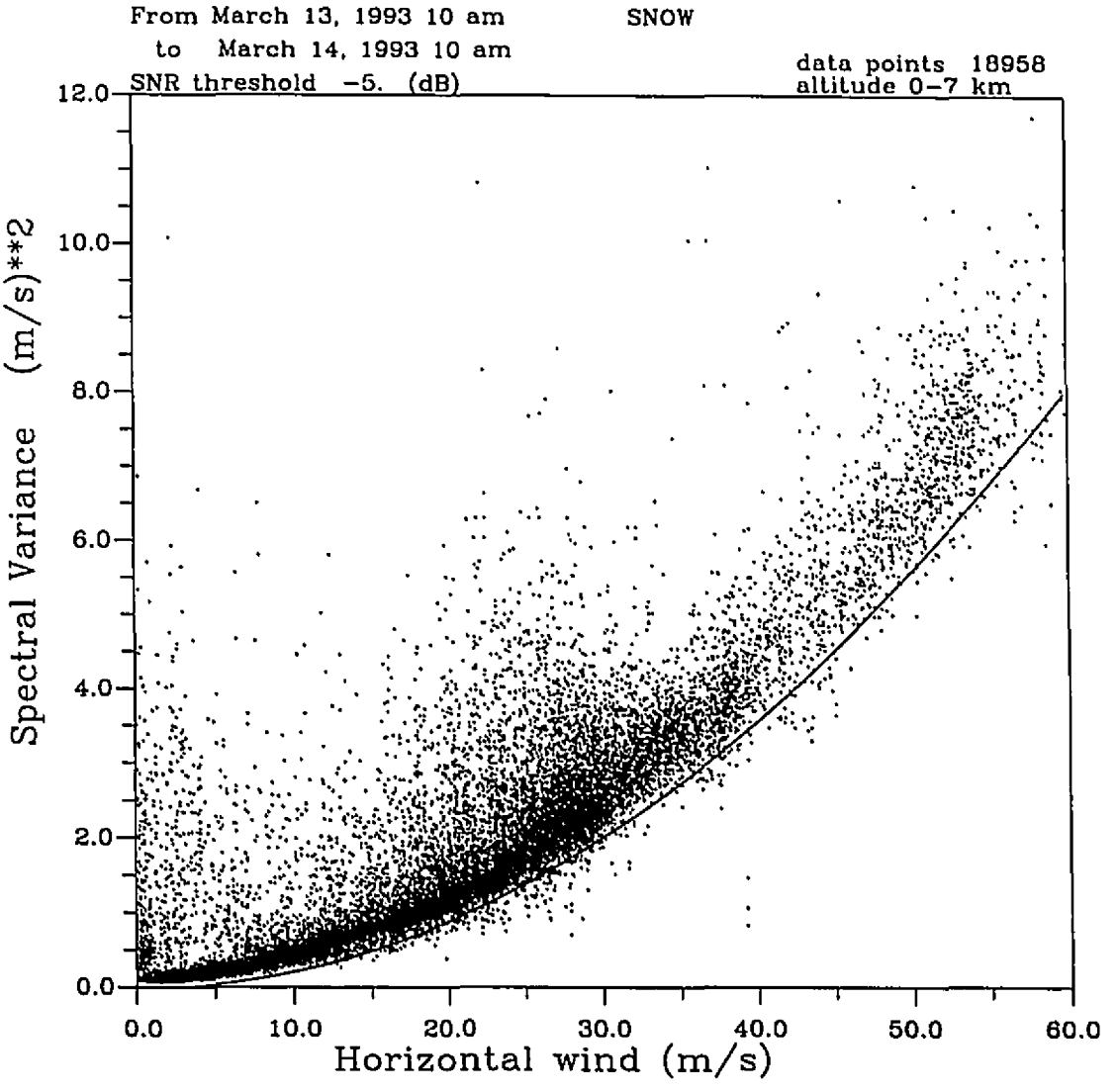

Figure 4.7: Spectral Variance vs Horizontal Wind

This is associated with the increasing wind speed. Figure 4.7 shows the theoretical contribution of the wind to the spectral variance, as plotted earlier in Fig 3.3, with the data from the storm.

Subtracting the variance due to the cross-beam wind component from the total spectral variance gives Fig. 4.8. This is a very important plot. Much of this thesis is based on interpreting the residual variance. There are three notable features on this figure. The first is the region above 3 km from 1500 to 2200 where the residual

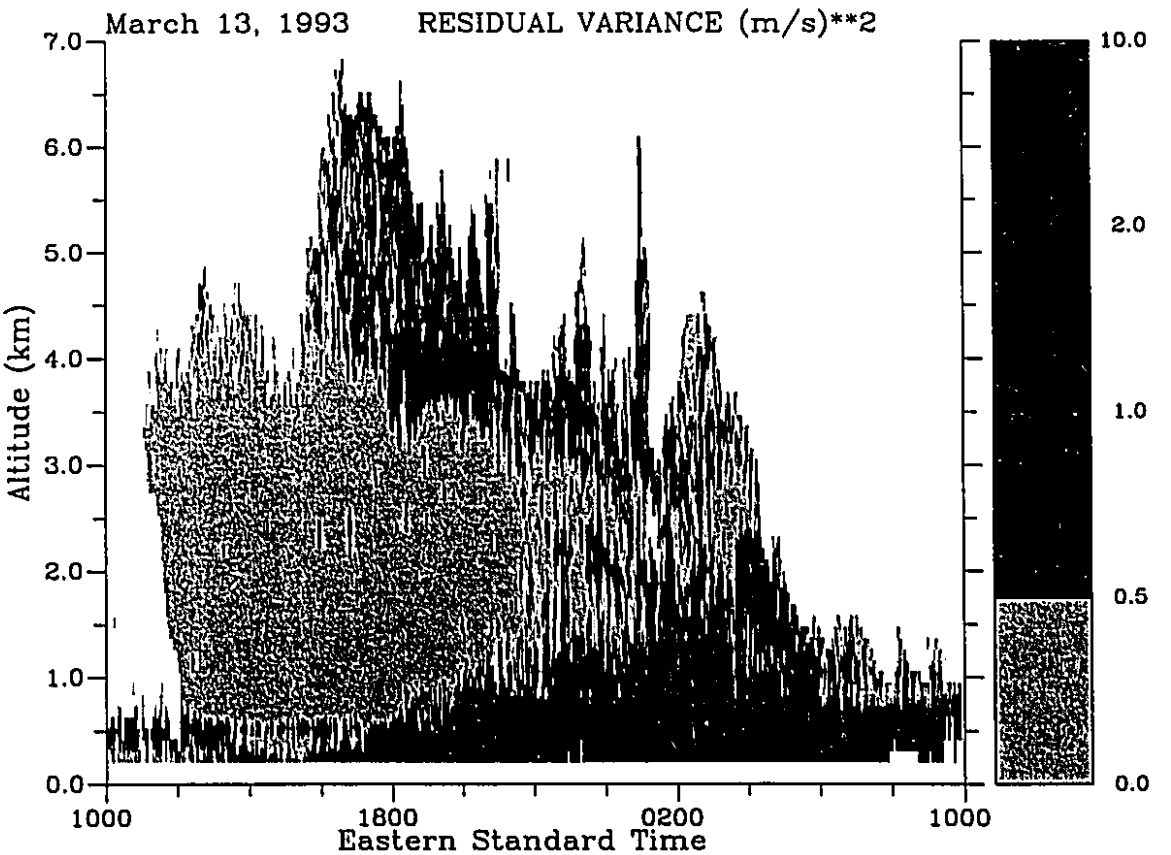

Figure 4.8: Residual Variance σ_r^2

variance is greater than 1 m^2s^{-2} . The second region of interest is below 1 km from 1700 to the end of the storm where there also are large values of the residual variance. The third feature is the remaining region of small values, less than 1 m^2s^{-2}. The calculation of the residual variance also gave some values less than zero, which are physically impossible. Those are the data that are below the theoretical line on Fig. 4.7 . Since they represent less than 2 % of the data, they have not been plotted on Fig 4.8 and are not used in any other calculation.

4.3 Wind Shear

Now that we have a field of residual variance, we must investigate the nature of this field. Is it really turbulence? A way to look for instability in the atmosphere is to examine the wind field for shear instability. The wind profiler gives us the horizontal vector wind as a function of altitude and time. The wind vector may be written

$$\mathbf{V}(z) = Ve^{i\theta}, \tag{4.2}$$

where $V = V(z)$ is the horizontal wind speed and $\theta = \theta(z)$ is the wind direction. The shear vector is

$$\frac{\partial}{\partial z}\mathbf{V}(z) = e^{i\theta}\left(\frac{\partial V}{\partial z} + iV\frac{\partial \theta}{\partial z}\right). \tag{4.3}$$

The magnitude of the shear vector is therefore

$$\left|\frac{\partial}{\partial z}\mathbf{V}(z)\right| = S_t = \sqrt{S_s^2 + S_d^2}, \tag{4.4}$$

where $S_s = \left|\frac{\partial V}{\partial z}\right|$ is the speed shear component and $S_d = V\left|\frac{\partial \theta}{\partial z}\right|$ is the directional shear component.

From the data, we can compute the total shear magnitude S_t, as well as the separate speed and directional components. For the computation we used the wind derived from 15-min consensus averages.

The speed shear at an altitude i was computed using the wind speed at the altitudes below and above ,

$$S_{si} = \left|\frac{|\mathbf{V}_{i+1}| - |\mathbf{V}_{i+1}|}{z_{i+1} - z_{i-1}}\right|. \tag{4.5}$$

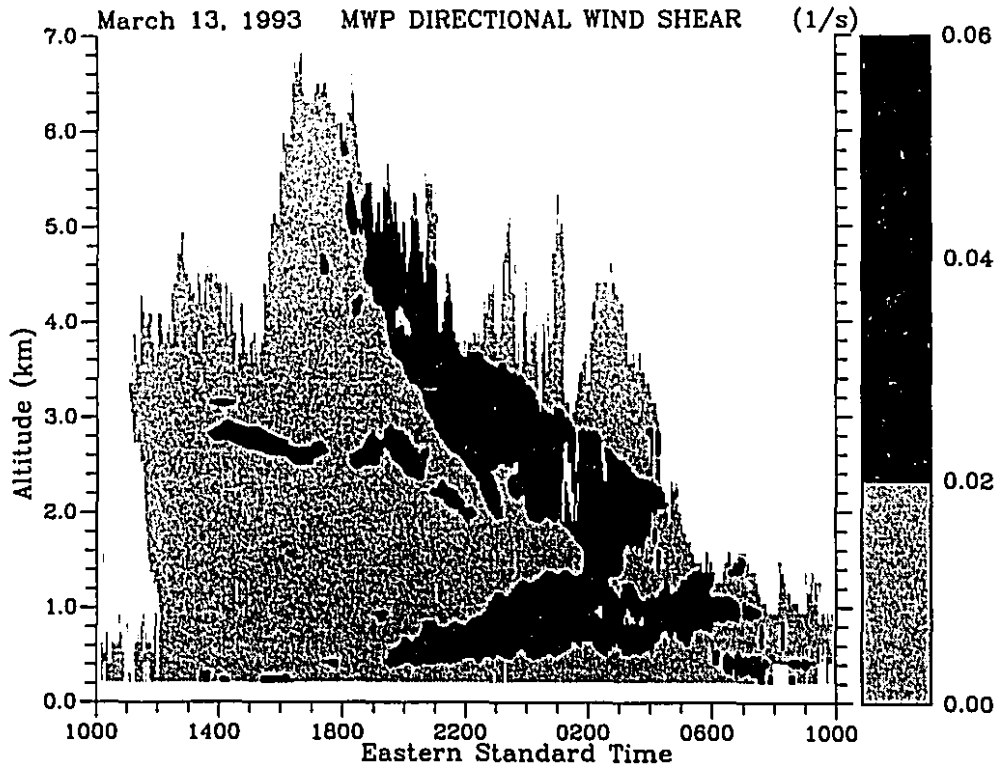

Figure 4.9: Directional Wind Shear

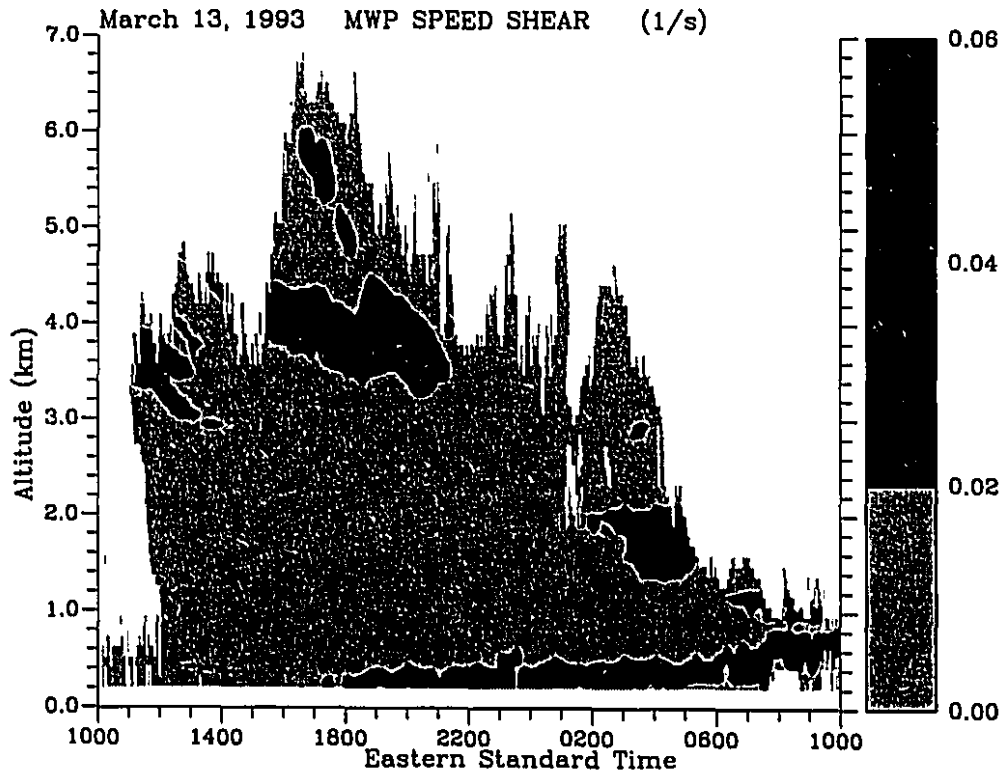

Figure 4.10: Speed Wind Shear

The total shear was computed by resolving the wind vector into its u and v components, and then calculating the change in these components with height, squaring and taking the square root of the sum.

$$S_{ti} = \sqrt{\left(\frac{u_{i+1} - u_{i-1}}{z_{i+1} - z_{i-1}}\right)^2 + \left(\frac{v_{i+1} - v_{i-1}}{z_{i+1} - z_{i-1}}\right)^2}. \tag{4.6}$$

The directional shear was computed from Eq. 4.4 as

$$S_{di} = \sqrt{S_{ti}^2 - S_{si}^2}. \tag{4.7}$$

Figures 4.9, 4.10 and 4.11 are respectively the directional, speed, and total shear fields. The directional wind shear in Fig. 4.9 has a well defined zone of importance, from 2000 on March 13, to 0800 on the 14. The structure is complementary to the speed shear pattern. The largest values of the speed shear can be found from 1600 to 2100 at altitudes above 3 km and below 1 km from 1400 to the end of the storm. Another region of strong speed shear is between 1.5 and 2.5 km for about 3 hours starting at 0100. The total wind shear, Fig. 4.11, has one major interesting feature. From 1600 at 4km there is a region of intense wind shear, which descends with time to 1.5 km the next day around 0300.

Comparing Figs. 4.9-4.11 with the pattern of residual variance in fig 4.8 shows that there is generally an association between regions of strong shear and regions of large residual variance. The association is closest with the pattern of total shear. This finding supports the interpretation of the residual variance as shear-induced turbulence.

An attempt to quantify the relation between the total shear and the residual variance was made. To examine that relation, blocks in time and in space were choosen in which large values of both σ_r and S_t were found. Those data are from

1500 to 2200 at altitudes above 3 km for the first block and from 1300 to 0800 at altitudes below 1 km for the second block. These blocks are indicated on Fig. 4.11.

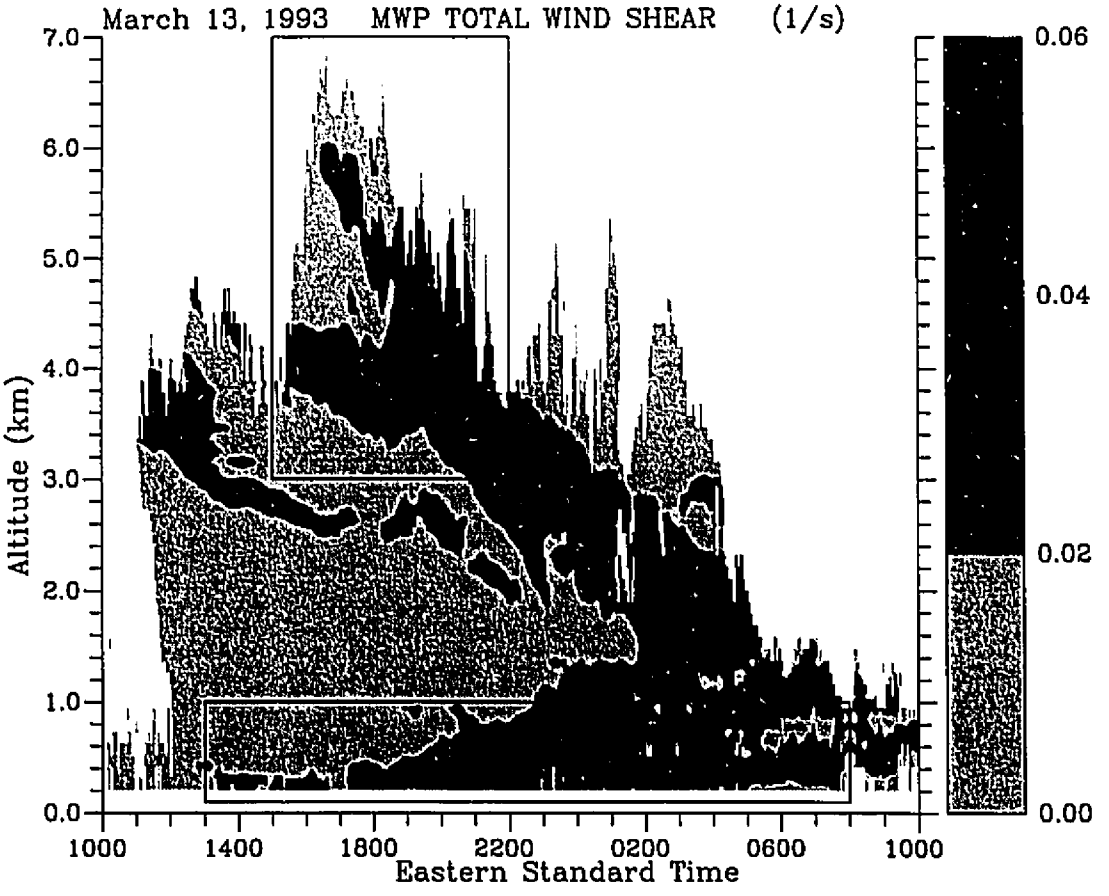

Figure 4.11: Total Wind Shear

We considered least-squares fits to the data of the form $\sigma_r = A + BS_t^C$ where C is a parameter that varied from 0 to 5. The best correlations were obtained with C close to 1.0, implying that the best fit is a linear one. The correlation coefficient found in block 1 was 0.20 with $A = 0.67$ and $B = 6.85$; Fig 4.12a shows that regression. For block 2, Fig 4.12b, $A = 0.38$ and $B = 26.36$ with a correlation coefficient of

a)

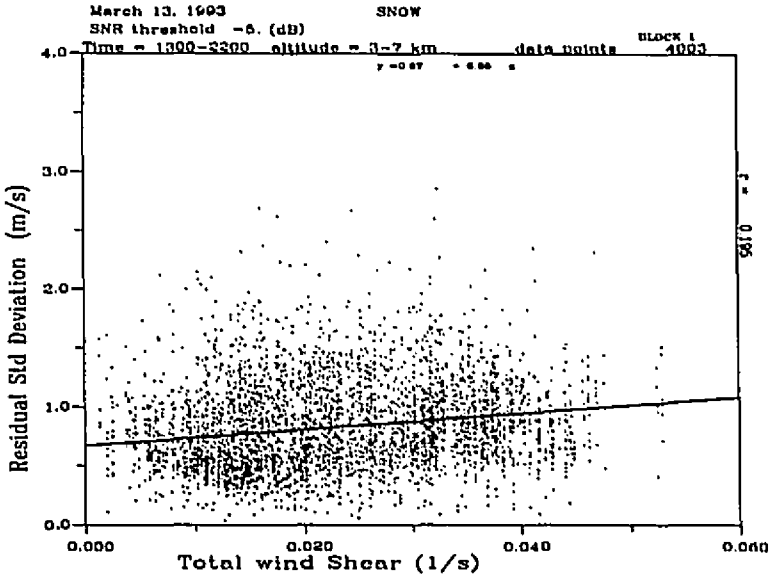

b)

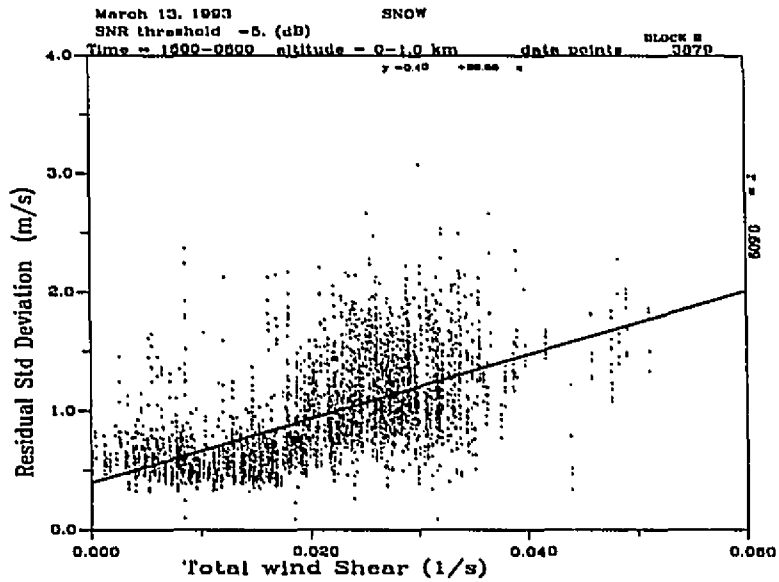

c)

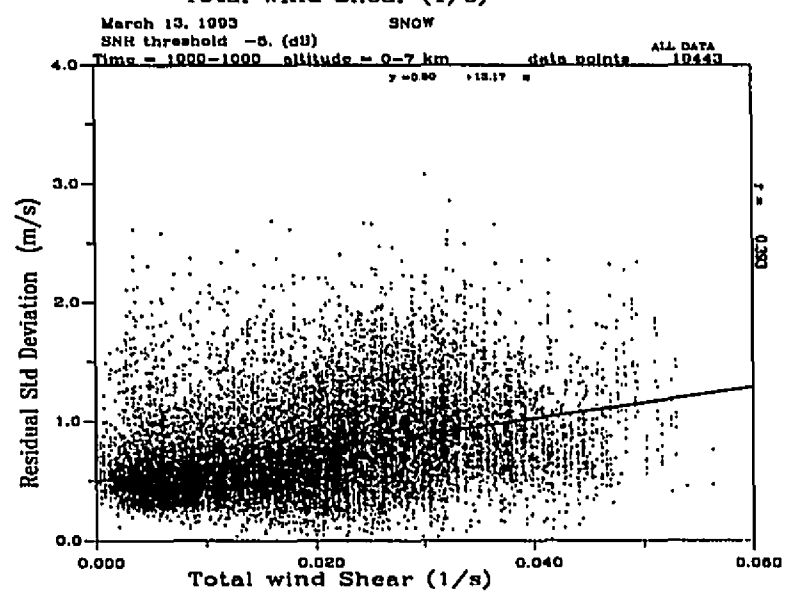

Figure 4.12: Scatter Plot of σ_r vs S_s a) From Block 1, b) From Block 2, c) From all the Data

0.67. And for the whole field (Fig. 4.12c) the results are $A = 0.50$, $B = 13.17$, and r = 0.40.

4.4 Large Scale Turbulence

So far we have examined turbulence through the quantity σ_r, the residual Doppler spread. This quantity indicates the strength of turbulent irregularities of scales generally smaller than the radar resolution volume. By looking at the variation in time of the mean vertical velocity $\bar{w}$ we can estimate the strength of the turbulence in eddies of scales larger than the resolution volume [19] , through the relation

$$\sigma_v^2 = < \bar{w}^2 > - < \bar{w} >^2 . \tag{4.8}$$

The average is done at every altitude of observations over periods of 30 min starting at 1000 on March 13. Figure 4.13 is the resulting field of σ_v^2 .

Most of the values, 99.3%, are less than 1 m^2s^{-2}. In fact, 63.3% of the values are less than 0.05 m^2s^{-2}. This is small but not unanticipated; Rogers and Tripp [19] wrote that 75 % of the energy resides in scales smaller than 100 m. If we add these values to the residual variance averaged over the same 30 min periods we can obtain the total turbulence intensity. Figure 4.14 is the σ_{Tot} field, defined by

$$\sigma_{Tot} = \sqrt{\sigma_v^2 + \sigma_r^2} \tag{4.9}$$

it is not much different from the pattern of residual variance in Fig. 4.8, because the values for the large scale turbulence are usually small compared to the small scale turbulence. We can again plot a scatter diagram versus the total shear. The result is very close to the plots of Fig. 4.12.

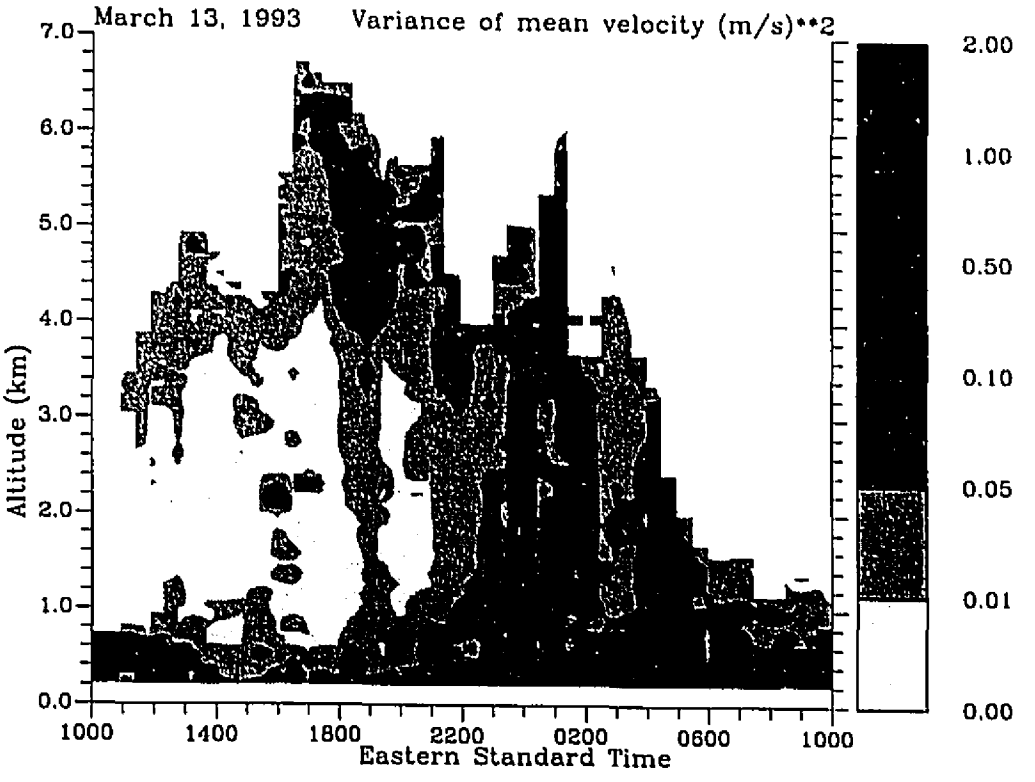

Figure 4.13: Large Scale Fluctuation Field

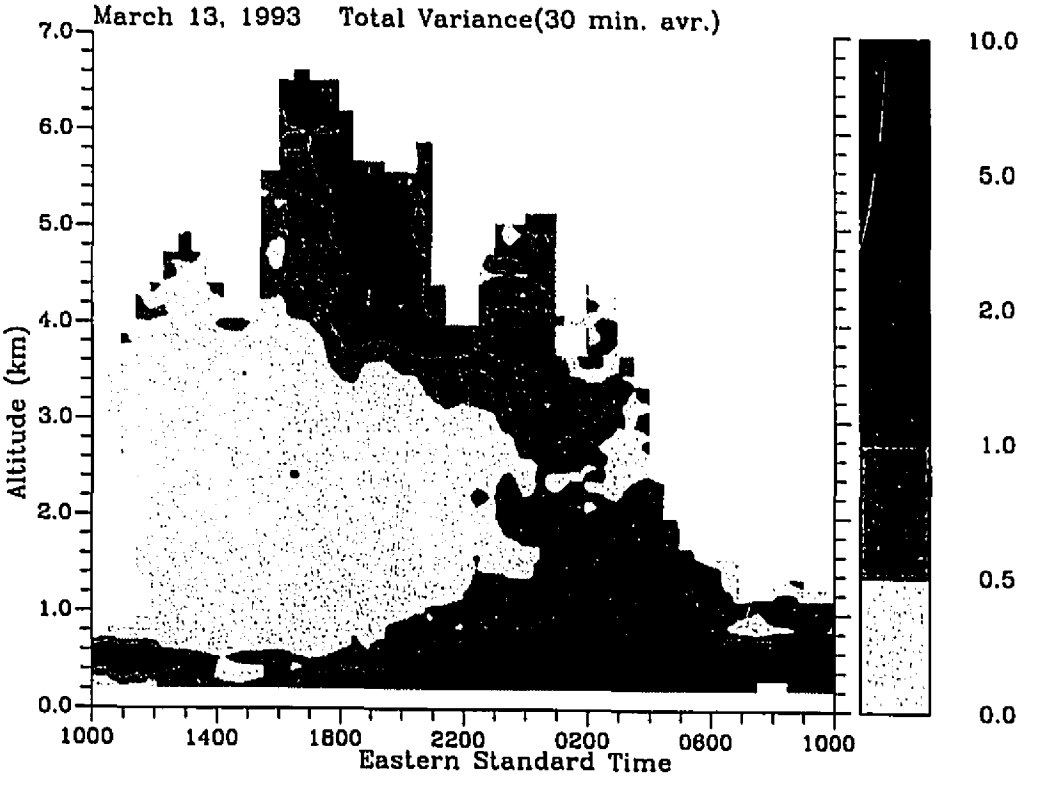

Figure 4.14: Total Variance Field

a)

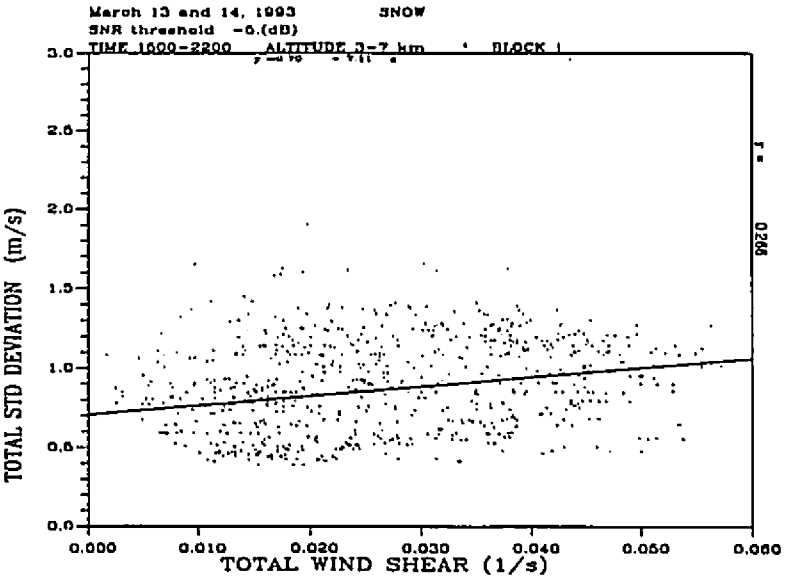

b)

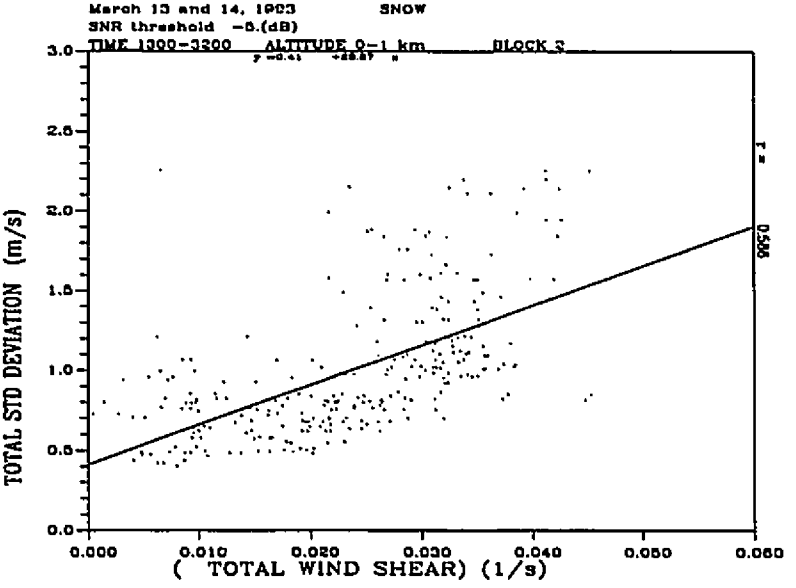

c)

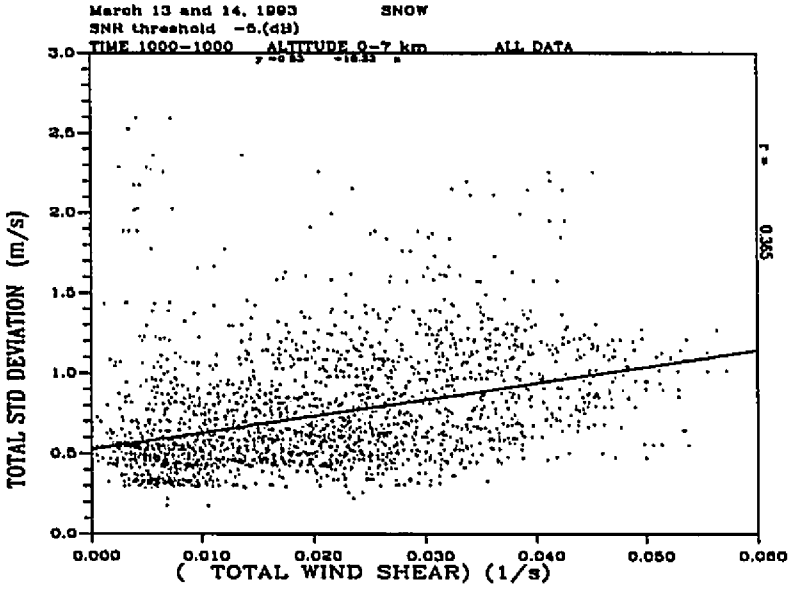

Figure 4.15: Scatter plot of σ_{Tot} vs total shear a) Block 1, b) Block 2, and c) all the data.

We have in Fig 4.15a a linear regression where $A = 0.70$ and $B = 7.11$ with a correlation coefficient of 0.27 for block 1. For the second block, in Fig 4.15b, we have $A = 0.41$ and $B = 29.87$ with a correlation coefficient of 0.59. The correlation between the total turbulence and the total shear is much better for block 2. For the complete field the regression gives $A = 0.53$ and $B = 12.33$ with a correlation of 0.37.

4.5 Richardson Number

To generate turbulence, a velocity gradient is required. We have that gradient in the form of wind shear. The static stability of the atmosphere counters the effect of this gradient. A measure of the relative importance of mechanical and density effects is the dimensionless Richardson Number :

$$Ri = \frac{N^2}{S^2} \tag{4.10}$$

where N is the Brunt-Väisälä frequency $[\frac{g}{\theta}\frac{\partial\theta}{\partial z}]^{1/2}$ and S is the wind shear. The Brunt-Väisälä frequency is a measure of the static stability of the atmosphere and the shear is a measure of the destabilizing effect of the wind [5]. Shear-induced pertubations are suppressed in regions where Ri is large. Therefore in regions where the small-scale turbulence is intense, we may expect to find small values of Ri. But to compute the Richardson number we need a temperature profile. Some choices are offered; one is to take a real sounding, but the nearest ones available are from Albany, N. Y. or Maniwaki, Quebec, both some distance from Montreal. VanZandt et al [23] used an average profile of temperature from twice-daily regular radiosonde from a nearby station over the six-days when their experiment was running. This gives a smooth profile of temperature. Another solution, the one used here, was to obtain

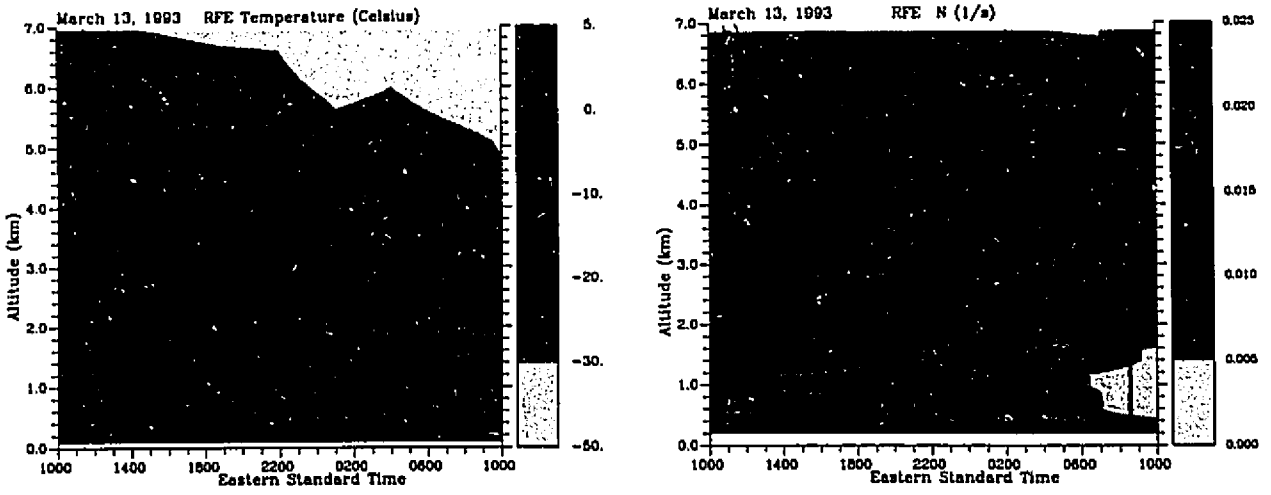

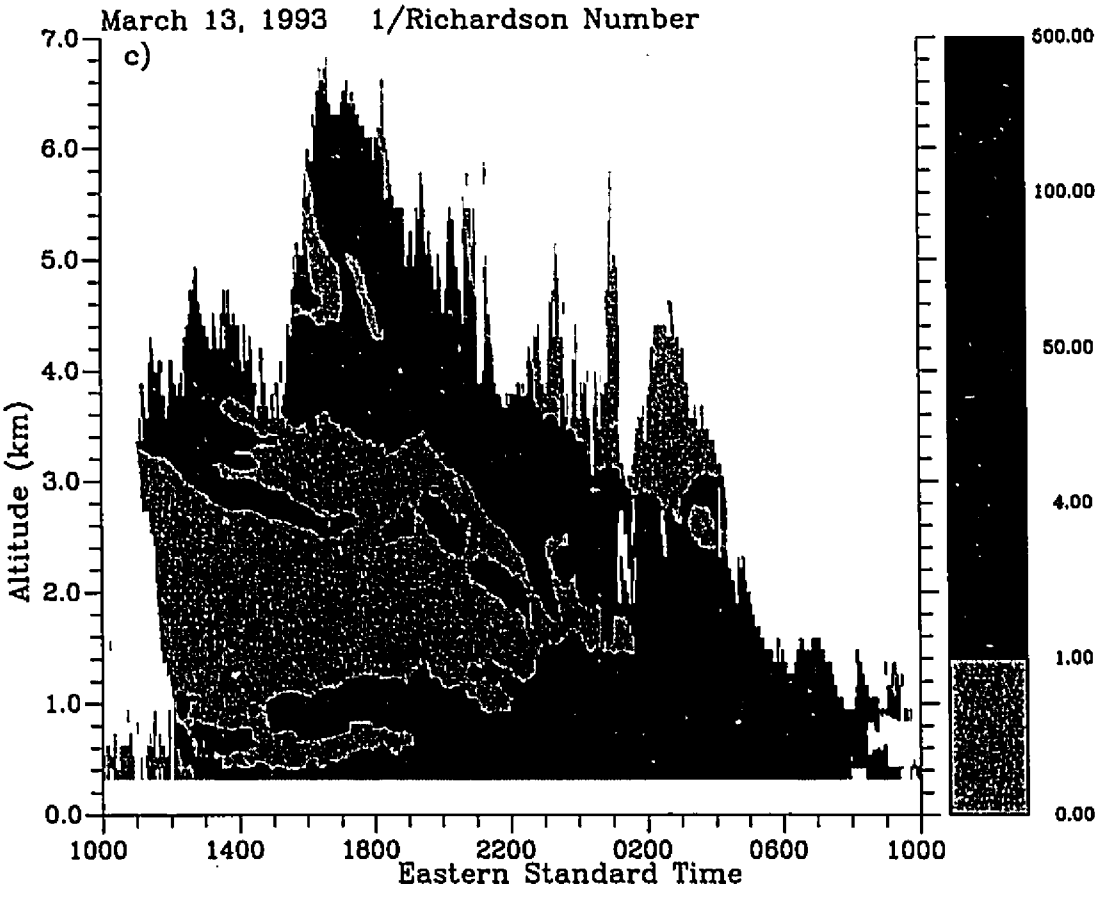

Figure 4.16: a) Temperature Field from RFE model, b) Brunt-Väisälä frequency based on RFE model, c) time-height pattern of $1/Ri$.

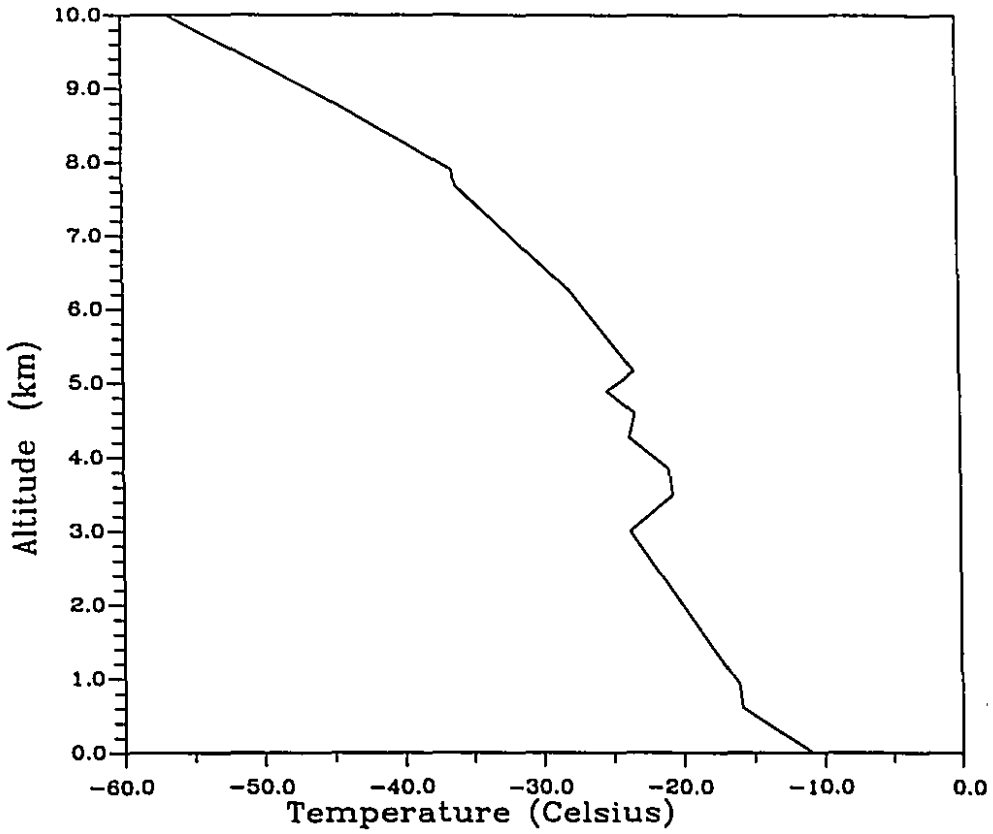

Figure 4.17: Temperature profile from Maniwaki, 1900 EST

temperature from a mesoscale numerical model. (See Appendix A for more details). Figure 4.16a shows the temperature field from the model for Montreal with a time resolution of 3 hours and a height resolution of 150 mb. Fig. 4.16b is the Brunt-Väisälä frequency. Altitudes above 5 km have absolute stability and some layers of saturated neutrality. There is an inversion at 3 km between 1400 and 2000. This is a real feature, consistent with the temperature profile from Maniwaki at 1900 (Fig 4.17).Fig. 4.16c is the field of Ri^{-1}, the reciprocal of Richardson number, which bears a close resemblance to Fig. 4.8.

a)

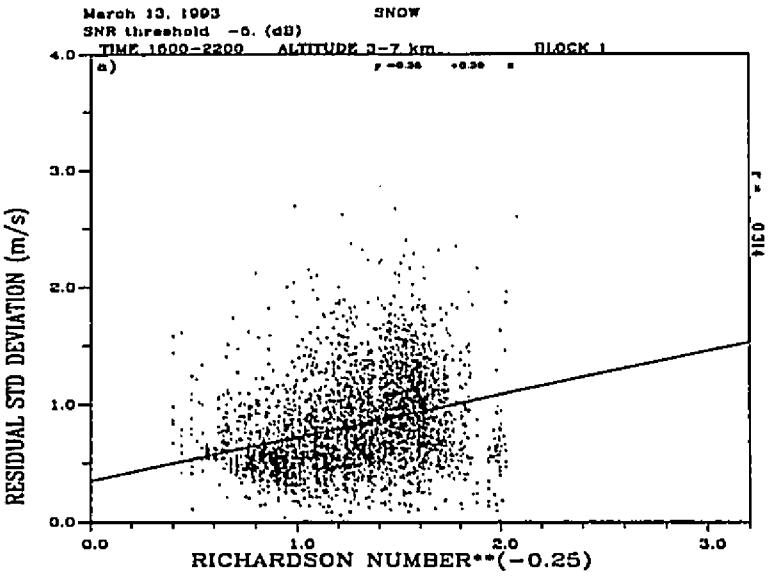

b)

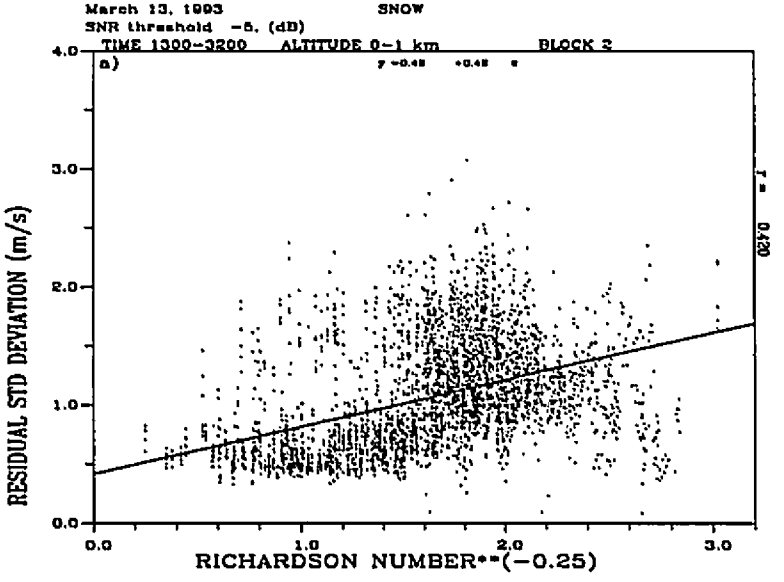

c)

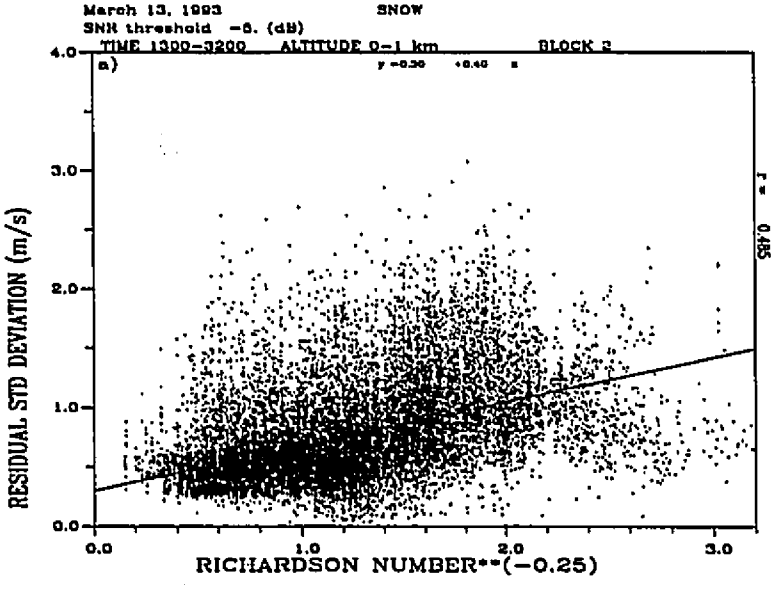

Figure 4.18: a) Linear Regression of σ_r vs $Ri^{-1/4}$ from Block 1, b) block 2, and c) all the data.

It seems appropriate to plot the reciprocal of the Richardson number, because this expands the dynamic range of the small values of Ri that are expected to be associated with turbulence. Here, we considered least-squares fits to the data of the form $\sigma_r = A + BRi^C$. The best values found for C were around -0.25. In region 1 we found the best fit $\sigma_r = 0.54 + 0.34Ri^{-0.25}$ with a correlation coefficient is 0.38. We can see this on Fig. 4.18a. A better fit is found for block 2, $\sigma_r = 0.42 + 0.42Ri^{-0.25}$ with a correlation coefficient of 0.42. For all the data, we have $\sigma_r = 0.30 + 0.40Ri^{-0.25}$ and $r = 0.49$.

Chapter 5

Energy Dissipation Rate

One way to quantify the turbulence is through the variance quantities considered earlier, σ_r^2, σ_v^2, and σ_{tot}^2. These are quantitive measures of turbulence intensity, but they depend on the parameters of the radar used to measure them. They depend on such quantities as pulse length and integration time. Another method, independent of the radar is the energy dissipation rate. The transformation of the residual variance into the energy dissipation rate ε is not straighforward. Hocking [14] has an estimation of the energy dissipation rate as

$$\varepsilon = 0.45\sigma_t^2 N \tag{5.1}$$

where σ_t^2 is the variance of the Doppler spectrum due to turbulence and N is the Brunt-Väisälä frequency. There are two important factors [14] that determine if Eq. 5.1 is appropriate. The radar resolution must be comparable to or larger than L_B, the outer scale of turbulence, and the integration time should be around a minute. Figure 5.1 is the field of ε computed using Eq. 5.1. There are two prominent areas where the values are greater than 100 cm^2s^{-3}, corresponding approximately to blocks 1 and 2 of Fig. 4.10.

But if the resolution of the radar is smaller than L_B and the integration time is in the order of a second we should use use the Frisch and Clifford [7] formula as

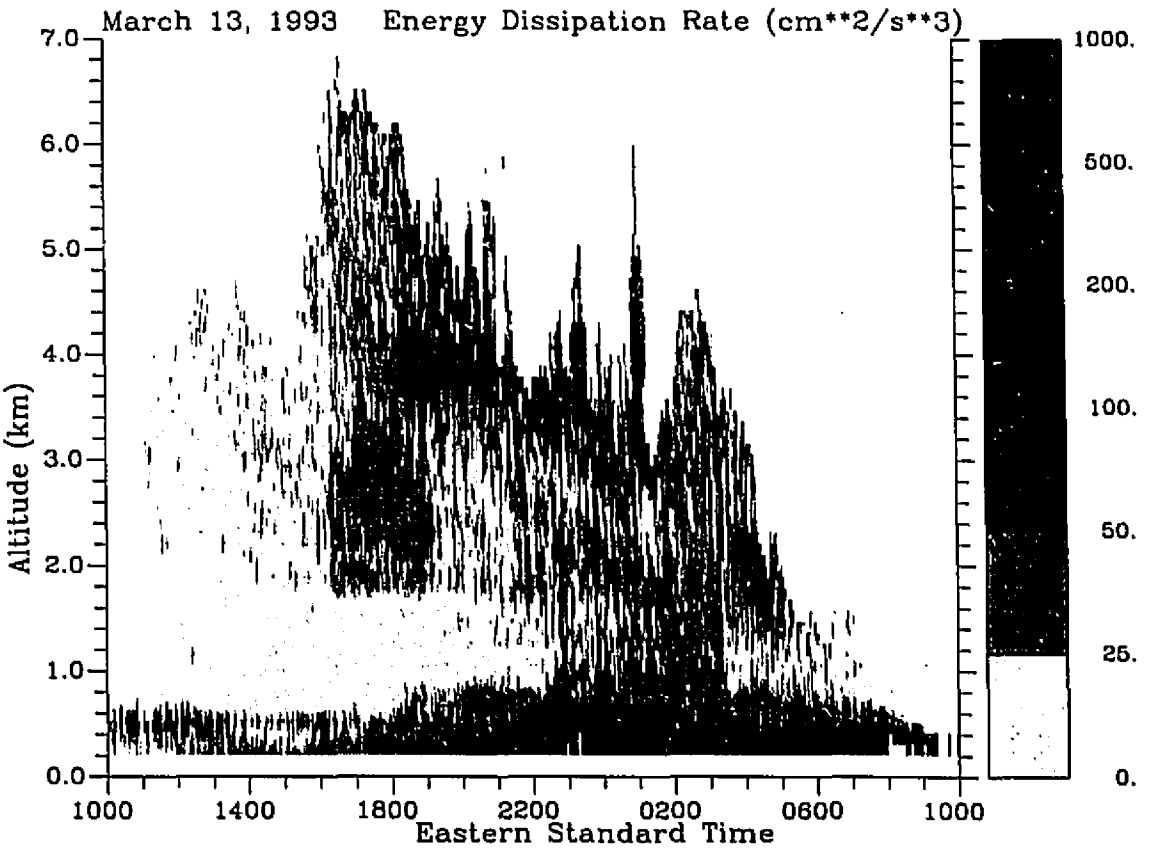

Figure 5.1: Energy Dissipation Rate (Hocking)cm^2s^{-3}

corrected by Bohne [2] :

$$\varepsilon = \frac{1}{\delta}\left[\frac{\sigma_t^2}{1.35A\left(1-\frac{\gamma^2}{15}\right)}\right]^{3/2} \tag{5.2}$$

where A is a constant, γ^2 is a parameter that depends on radar pulse length and beamwidth, and δ is a parameter that depends on range, pulse length, and beamwidth. Specifically,

$$\left.\begin{aligned}\delta &= \alpha \\ \gamma^2 &= 1-\left(\tfrac{\beta}{\alpha}\right)^2\end{aligned}\right\} \text{when } \beta \le \alpha \tag{5.3}$$

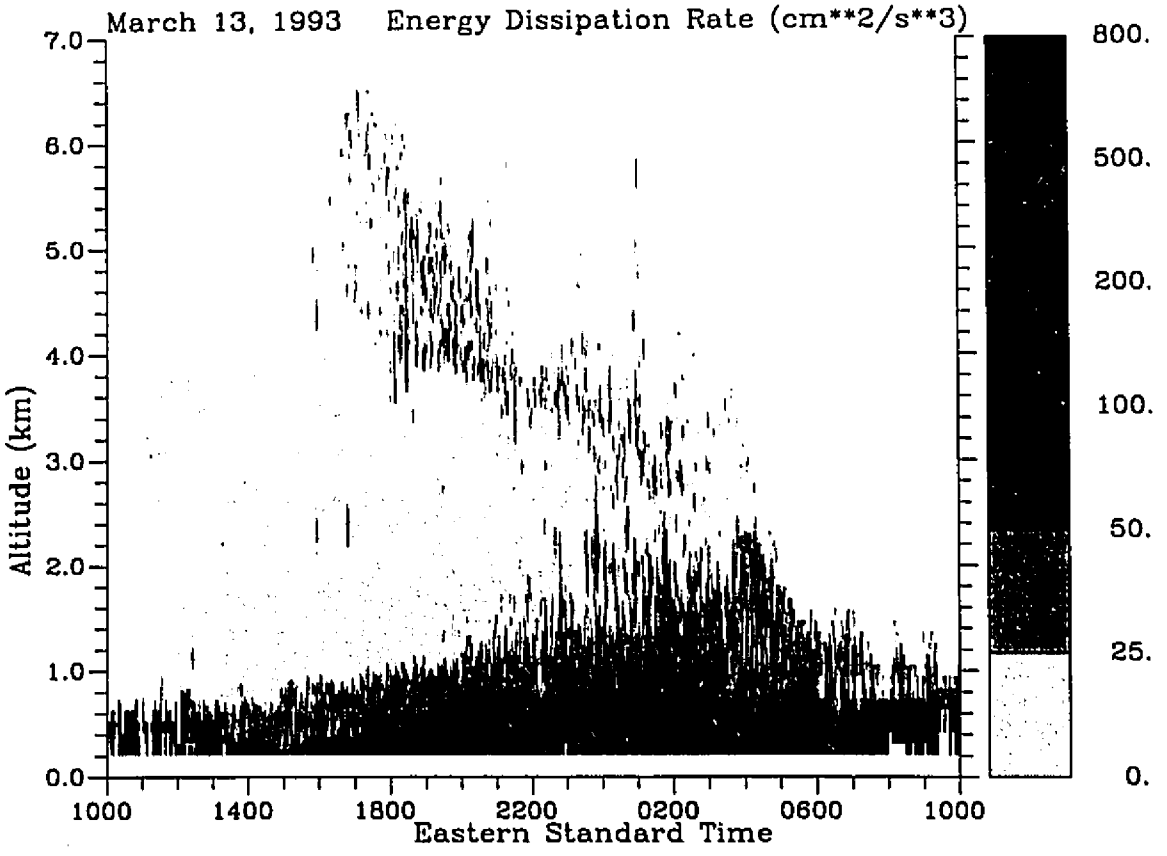

Figure 5.2: Energy Dissipation Rate (Frisch & Clifford)cm^2s^{-3}

$$\left.\begin{aligned} \delta &= \beta \\ \gamma^2 &= 4\left[1-\left(\tfrac{\alpha}{\beta}\right)^2\right] \end{aligned}\right\} \text{when } \beta > \alpha \qquad (5.4)$$

where, for the Montreal Wind Profiler β = 44m and α = 0.066R where R is the radial distance. Thus, (5.3) is the appropriate relation for $R \geq 667m$ and (5.4) is appropriate for closer ranges. Bohne [2] gives 1.35 for the value of A, but Gossard et al [9] indicate that its value ranges from 1.53 to 1.68. Vincent and Meneguzzi [24] did obtain, with a model, a value of 2. A value of 1.6 seems to be a good compromise. Fig 5.2 is the field of ε computed with the Frisch & Clifford equation. There is one region, below 1 km, where the values for ε are greater than 100 cm^2s^{-3}.

The difficulty with our observations is that the averaging time and the radar resolution are larger than appropriate for the Frisch and Clifford theory and smaller than appropriate for the Hocking theory. The outer scale L_B cannot be obtained directly from our observations, but Weinstock [26] has shown that L_B can be written as

$$L_B = \frac{2\pi}{0.62}\varepsilon^{1/2}N^{-3/2} \tag{5.5}$$

which applies for shear generated turbulence in statically stable regions. By using Eq. 5.1 or Eq. 5.2 we can obtain values of ε, which can be combined with N determined earlier (see Fig 4.16) to yield L_B. Figure 5.3 contains two averaged profiles over a 24-hour period of L_B based on Eq 5.5. Profile *a* was computed with Eq. 5.1 and profile *b* with Eq. 5.2.

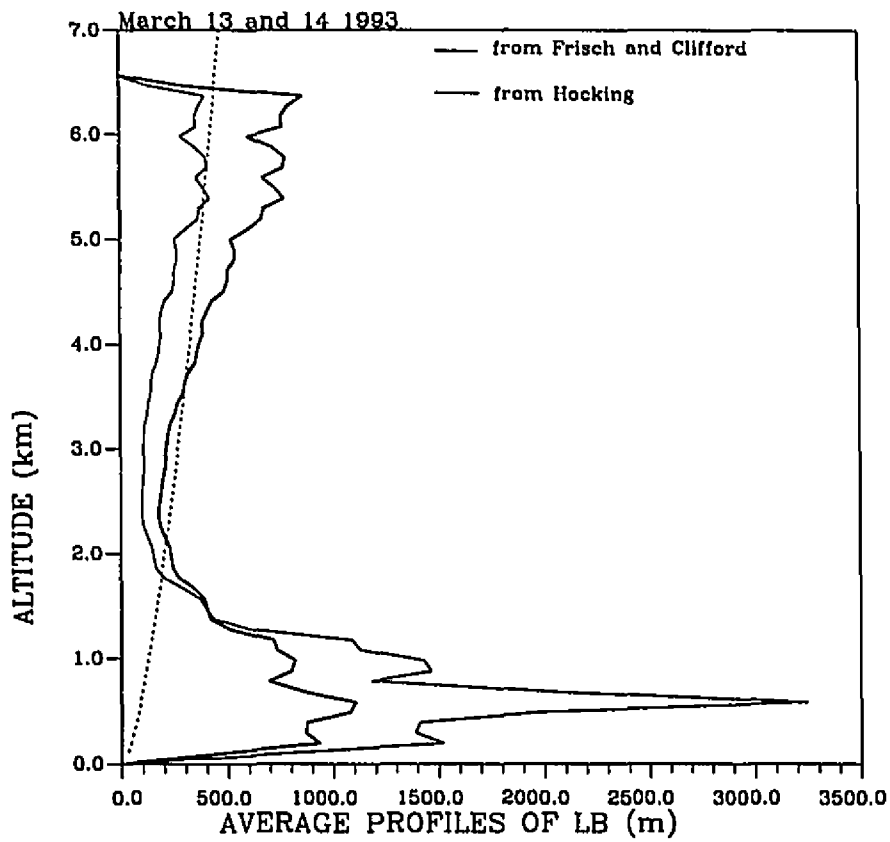

Figure 5.3: Average Profile of L_B based on a) ε from Hocking , b) ε from Frisch & Clifford. The dashed line is the effective linear dimension of the radar sampled volume.

The vertical resolution of the radar for these observation is 105 meters. The horizontal resolution varies with height as $r = 0.16R$. The effective linear dimension of the radar resolution may be taken as the cube root of the resolution volume. This function is the dashed line on Fig 5.3. This figure shows that regardless of how the outer scale is computed, and for all altitudes except the interval between approximately 2 and 4 km, the outer scale is comparable to or larger than the radar resolution volume. Consequently we conclude that the Frishch-Clifford theory is the more appropriate one for our observations and Fig 5.2 is the more accurate picture of the energy dissipation rate.

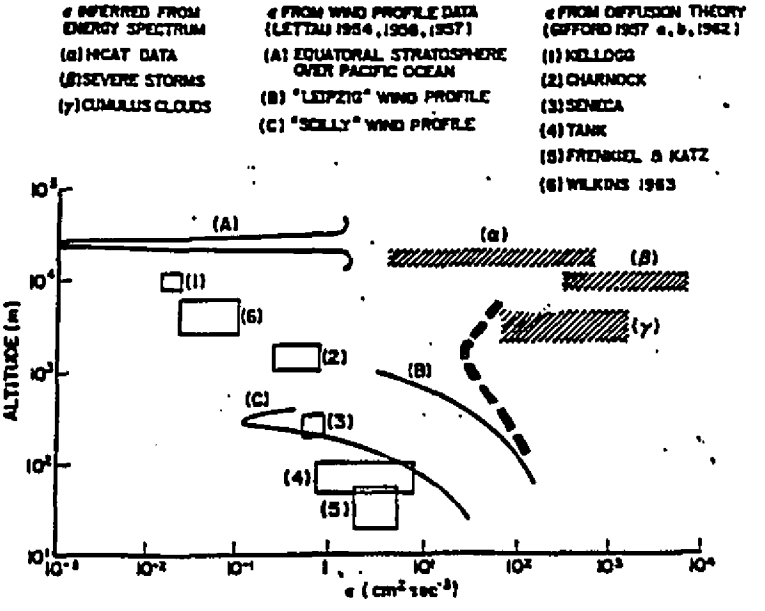

Figure 5.4: Samples of the energy dissipation rate

Figure 5.4 [4] shows measurements of ε reported by others over a range of altitudes. The dashed line is the average profile during the Storm of the Century. The data from the profiler are within the normal ranges. They are somewhat higher than the "Leipzig" wind profile and within the range of values for cumulus cloud. The values for ε inferred from energy spectrum, namely the Hicat Data (α) , severe storms (β) , and cumulus cloud (γ) were also calculated from spectral variances. The

values found with the Montreal Wind Profiler are bigger then the ones on Fig 5.4 for altitudes below a kilometer, probably because of the strong low-level wind and wind shear.

Chapter 6

Clear air

6.1 Turbulence and clear air echoes

The Montreal Wind Profiler very often detects layers of clear-air echoes. The radar measures reflection that depends on both the strength of the turbulence and the spatial variability of the refractive index [6]. This index depends on the potential temperature, the pressure and the humidity. In Chapter 3, we saw how to estimate turbulence in precipitation from the Doppler spectrum. This can also be used in clear air, except that the broadening from differential fall speed becomes irrelevant here. What we called the residual variance is now the variance due to turbulence :

$$\sigma_t^2 = \sigma_r^2 = \sigma_s^2 - \sigma_w^2. \tag{6.1}$$

In this chapter, the symbol σ_t^2 will be used for the theory, and σ_r^2 for the data. The goal of this chapter is to compare the reflectivity of clear air with the residual variance. Both quantities are related to turbulence.

6.2 Comparison of Z and σ_t^2

A simple way to find a relation between the reflectivity Z and σ_t^2 is from Tatarskii [25], assuming a thin layer where the turbulence is isotropic and homo-

geneous

$$C_n^2 = a^2 L_B^{4/3} M^2 \tag{6.2}$$

where C_n^2 is a structure parameter describing the strength of refractivity fluctuations, M is the mean vertical gradient of generalized potential refractive index, L_B is the outer scale of turbulence, and a is a universal constant. Also

$$L_B^{4/3} \propto \overline{\Delta v^2} \tag{6.3}$$

or

$$L_B \propto \overline{\Delta v^2}^{3/4} \tag{6.4}$$

We also have

$$\overline{\Delta v^2} \propto \sigma_t^2 \tag{6.5}$$

and

$$Z \propto C_n^2 \tag{6.6}$$

Thus

$$Z \propto C_n^2 \propto \overline{\Delta v^2} \propto \sigma_t^2 \tag{6.7}$$

It means that we should expect

$$Z \propto \sigma_t^2 \tag{6.8}$$

for a thin atmospheric layer. This proportionality can also be demonstrated by using Eq. 5.2 :

$$\varepsilon = \frac{1}{\delta}\left[\frac{\sigma_t^2}{1.35A\left(1-\frac{\gamma^2}{15}\right)}\right]^{3/2} \tag{6.9}$$

and from Hocking [14]

$$C_n^2 = \frac{0.7F^{1/3}}{N^2}\varepsilon^{2/3}M^2, \tag{6.10}$$

where F = fraction of the beam filled with turbulence

N = Brunt-Vaisala frequency

M = gradient of refractive index

We can convert C_n^2 in terms of the reflectivity Z using from Rogers et al [18]

$$C_n^2 = 7.49 \times 10^{-16} \lambda^{-11/3} Z \tag{6.11}$$

where C_n^2 is in $m^{-2/3}$, Z is in $mm^6 m^{-3}$, and λ, the wavelength of the profiler is in m. For the wavelength of 33 cm, the relation 6.11 becomes

$$C_n^2 = 4.46 \times 10^{-14} Z. \tag{6.12}$$

Combining Eq 6.9, 6.10, and 6.11 we have

$$Z = \frac{0.7F^{1/3}}{4.46 \times 10^{-14} N^2} \left(\frac{1}{\delta}\right)^{2/3} \frac{M^2 \sigma_t^2}{1.35A\left(1 - \frac{\gamma^2}{15}\right)}. \tag{6.13}$$

Considering a thin layer of the atmosphere, the right hand side of Eq 6.13 becomes proportional to σ_t^2. Thus

$$Z \propto \sigma_t^2 \tag{6.14}$$

6.3 Data Analysis

6.3.1 Method 1: Direct Analysis

Three different days were chosen for the study of clear air. Since the results for those days are similar, only the data for July 6, 1993 will be described with the direct approach. Let us first have a look at all the data for a twelve-hour period without precipitation, from 0400 to 1600 hrs. To avoid ground clutter we used only the data above 1000 m. Fig. 6.1a is a plot of the spectral variance versus the horizontal wind for July 6.

a)

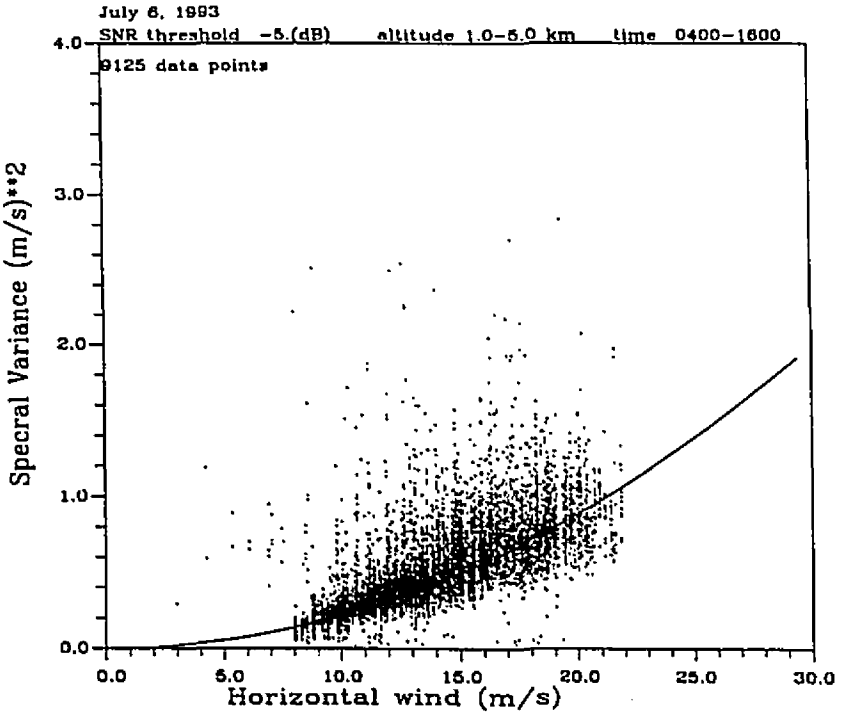

b)

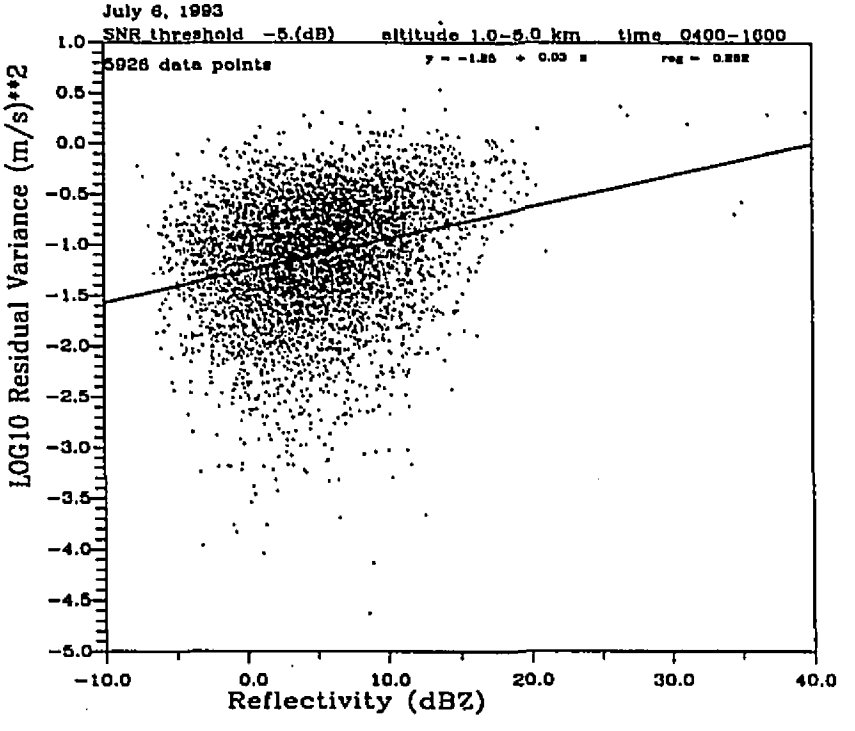

Figure 6.1: Clear Air data. July 6, 1993 a) Spectral Variance vs Horizontal Wind with the theoretical curved for the broadening of the spectrum by the wind (Eq. 3.3) b)$\log_{10}$(Residual Variance) vs Reflectivity with linear regression.

The line is the theoretical curve for the contribution of the horizontal wind to the spectral variance (Eq. 3.3). We saw a similar plot for the March 13, 1993 snowstorm in Chapter 4 (Fig. 4.7). In that plot, only 2 % of the data were below the theoretical curve. Here, however, the residual variances are smaller and 35% of the data are below the theoretical curve. Those data correspond to negative residual variance. They are not used in this section. From Eq 6.8 and Eq 6.14 we expect a linear relation between Z and σ_t^2 if all other factors such as L_B and M are constant. A plot of $\log_{10}\sigma_t^2$ vs the reflectivity factor is shown on Fig 6.1b. A linear regression was made on that scatter plot. The regression is $\log_{10}\sigma_t^2 = -1.25 + 0.03dBZ$. This gives the following relation

$$\sigma_t^2 = 0.06Z^{0.3} \tag{6.15}$$

It is too much to expect to find $\sigma_t^2 \propto Z$ for a range of 3 km in altitude and 12 hours in time because of the variability in height and time of M and L_B. Separating height into intervals of 500 m should give regions where those variables are more constant.

The first region is from 1000 m to 1500 m in height. In that layer we have a similar proportion of negative values for σ_r^2: 31 %. Table 2 shows the percentage with height

Table 2. Clear Air data, July 6, 1993	
Height(m)	% of negative residual variance
1000-1500	31
1500-2000	22
2000-2500	48
2500-3000	61
3000-3500	60
3500-4000	63

Figure 6.2 contains plots like Fig. 6.1a, but with only the data from 1000-1500 m for

a)

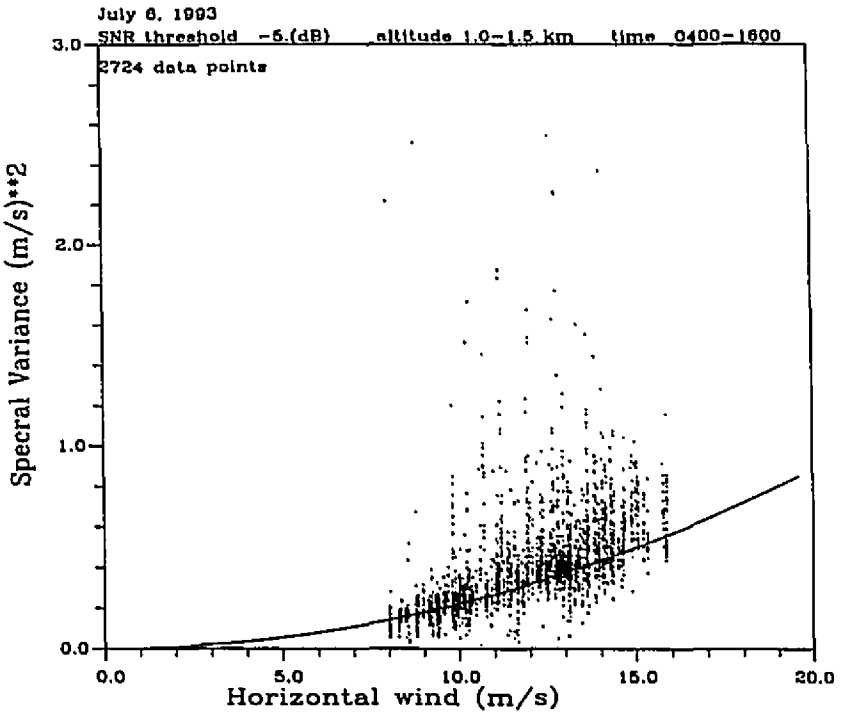

b)

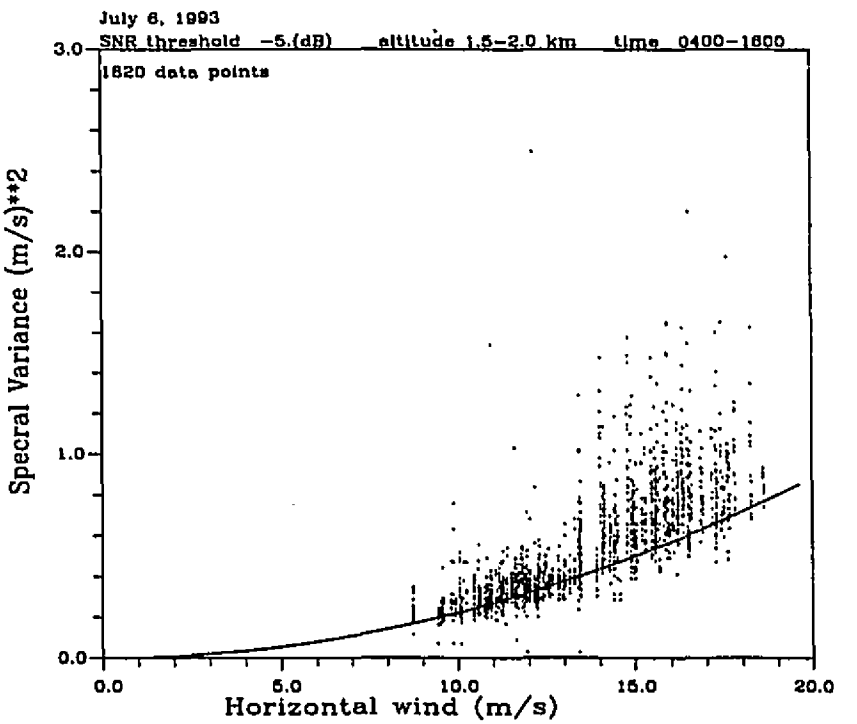

Figure 6.2: Clear Air Data. Spectral Variance vs Horizontal Wind for a) 1000-1500 m b) 1500-2000 m

a)

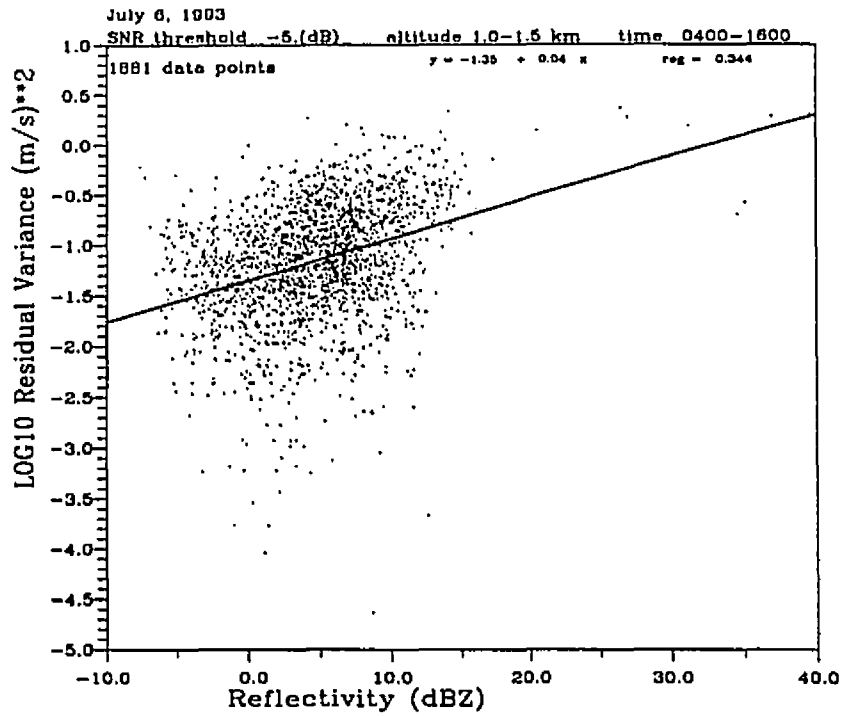

b)

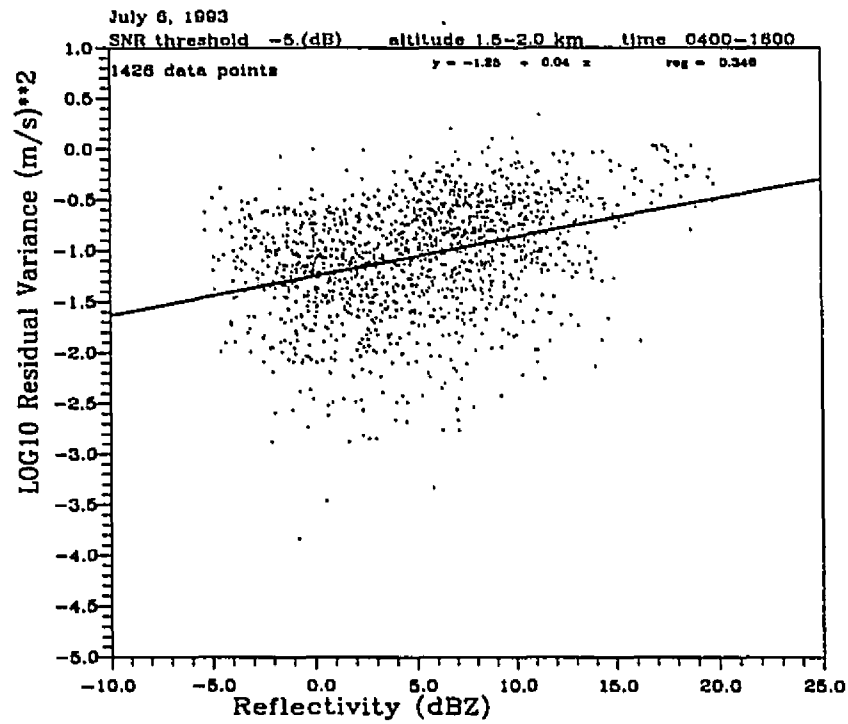

Figure 6.3: Clear Air Data. July 6,1993. $\log_{10}$(Residual Variance) vs Reflectivity a) 1000-1500 m b) 1500-2000 m

a and 1500-2000 m for b. These intervals are where the data seem to be closer to the theoretical curve for the broadening of the spectrum by the horizontal wind. These are the regions where the data follow a similar relation as Eq. 6.14. The relation found there is $\sigma_r^2 \propto Z^{0.5}$. Figure 6.3 contains the scatter plots for these two regions. Table 3 contains the exponent for Z and the correlation coefficient found for each layer. However, choosing a different part of a layer in time can give different result. Using data from 1500 to 1900 m and from 0400 to 0700 hrs gives an exponent of -0.04.

Table 3. Clear Air data, July 6, 1993		
Height(m)	exponent	r
1000-1500	0.4	0.34
1500-2000	0.4	0.35
2000-2500	0.1	0.09
2500-3000	-0.6	0.09
3000-3500	-1.0	0.43
3500-4000	0.02	0.01

6.3.2 Method 2: Average of σ_r^2

To apply Method 1, we had to reject a lot of data because they did not seem to have a physical meaning since the variance cannot be negative. Another way to examine the data is to take the average of all the residual variances, positive and negative, over ranges of values for the reflectivity. We averaged the residual variance over intervals of 10 dBZ and ploted it versus the median of the range. We saw earlier that the relation expected between σ_t^2 and Z is linear. A weighted regression based on the number of data points used to do the average was done between $\log_{10} \overline{\sigma_r^2}$ and dBZ for each of the three days at intervals of 500 m. Fig 6.4 is the weighted linear regression for the three lowest altitude ranges for July 6, 1993. From the linear regression we can find a relation

$$\sigma_r^2 = AZ^B \tag{6.16}$$

a)

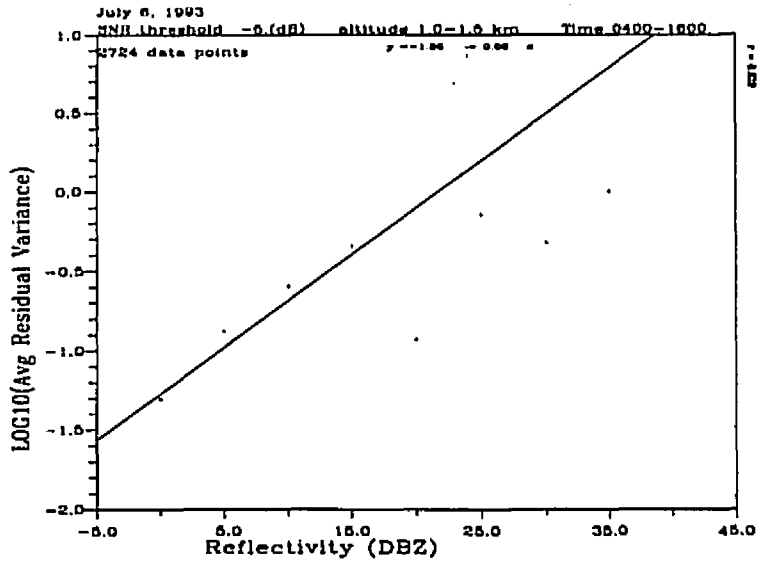

b)

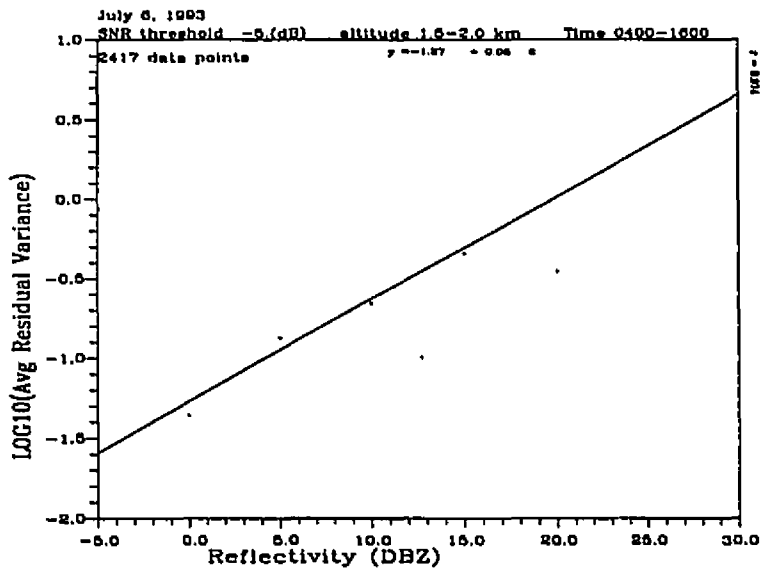

c)

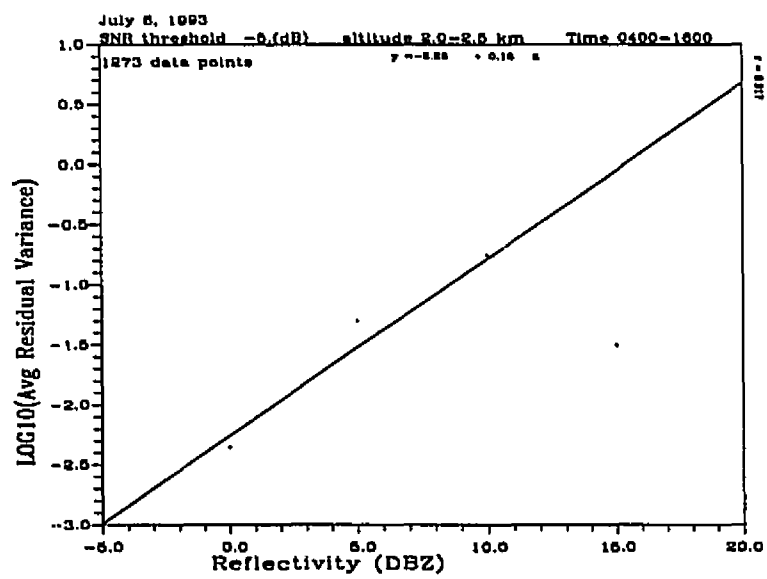

Figure 6.4: Clear Air Data. July 6,1993.Scatter Plot with weighted linear regression of $\log_{10}$(Average Residual Variance) vs Reflectivity a) 1000-1500 m b) 1500-2000 m, c) 2000-2500 m.

where the exponent B is 10 times the slope of the weighted regression. Table 4 shows the exponent found for July 6, 1993. The theory says that the exponent should be one. The table indicate values of 0.6 and 1.5 for the exponent, which may be taken as reasonably close to theoretical expectation.

Table 4. Clear Air data, July 6, 1993		
Height(m)	exponent	data points
1000-1500	0.6	2724
1500-2000	0.6	2417
2000-2500	1.5	1273

However, the exponents found for June 25, 1993 are far from the theory. Table 5 shows positive and negative values for the exponent.

Table 5. Clear Air data, June 25, 1993		
Height(m)	exponent	data points
1000-1500	0.2	1499
1500-2000	-0.1	621
2000-2500	0.1	592
2500-3000	-0.9	93
3000-3500	-1.6	22

Finally the data from July 9, 1993 also disagree with theory. That day gives positive and negative exponents. The two to altitude ranges have values close to the theory, but with very few data points.

Table 6. Clear Air data, July 9, 1993		
Height(m)	exponent	data points
1000-1500	-0.4	1375
1500-2000	-0.1	1295
2000-2500	-0.3	666
2500-3000	0.6	561
3000-3500	0.7	273
3500-4000	1.0	174

Most of the height intervals show a positive value for the exponent of Z, but not a value close to 1. This shows that an equation of the form of 6.16 may approximate the data, but the exponent B is generally less than 1. On the average for the three days, $B = 0.4$.

Chapter 7

Discussion and Conclusions

The main objective of this research was to measure turbulence with a small wind profiler. This was done using data from a large and intense snowstorm by subtracting the contribution of the cross-beam wind to the spectral variance measured in the vertical beam. The values for the resulting variance, the so-called residual variance, look reasonable; only 2 % of the data give negative values, 27 % of the values were greater than 1 m^2/s^2 for block 1 and 52 % for block 2. This corresponds to values around 100 cm^2s^{-3} in terms of energy dissipation rate for block 1, and values greater than 500 m^2/s^2 for block 2. It was also found that the contribution of the turbulence with scales larger than the radar resolution to the total turbulence is small compared to that of scales less than the radar resolution.

By comparing the residual variance to the wind shear, it was found that the turbulence is more closely associated with the total shear than with the speed or directional shear. A linear fit between the total shear and the residual standard deviation gave $\sigma_r = 0.70 + 7.11S_s$ for block 1 and $\sigma_r = 0.41 + 29.87S_s$ for block 2. Looking at another storm with less intense wind did not reveal as strong a relation between the total shear and the turbulence as for the storm of the century.

A calculation of the Richardson number was done using temperature profiles from a mesoscale numerical model and the total wind shear. In block 1, 94 % of the

values of $\frac{1}{Ri}$ were less than 1, and 96 % in block 2. This shows that the stability of the atmosphere is small in those regions. The best relations found between Ri and σ_r were $\sigma_r = 0.35 + 0.39Ri^{-1/4}$ for block 1, and $\sigma_r = 0.42 + 0.42Ri^{-1/4}$ for block 2.

A similar analysis was applied to clear-air echoes, to look for a relation between reflectivity and turbulence intensity. It was found that there is a tendency for the residual variance to increase with reflectivity, but not at the rate expected from a simple theoretical argument which predicts $\sigma_t^2 \propto Z$. On the average we found that the residual variance was proportional to $Z^{0.4}$, though there was much variability about this relation. The discrepancy may be explained by partial beam filling, which is more likely for thin, clear-air reflective layers than for snow. Also the signal is generally weaker during clear air days, giving more potential for noise influence.

Future research should include more snow cases to see if the dependence between the speed shear and the turbulence holds, as well as more clear air cases with stronger echoes and greater vertical extent to reduce the importance of noise effects and partial beam filling.

Appendix A

RFE Model

The temperature profiles used in this research came from a new version of the Regional Finite Element (RFE) model[16] used by the Canadian Meteorological Center (CMC). It was used by Z. Huo, a Ph.D student in this department, to provide a high-resolution and more realistic four dimensional dataset for the study of the deepening mechanisms associated with the March 13 and 14 , 1994, snowstorm. Here is a table of the initial data given by the model. They were linearly interpolated to be on same time and height as the data from the wind profiler. The model gave a profile each three hours.

time = 15 Z		
Height (dm)	Temperature (c)	Potential Temperature (K)
906.17	-39.10	330.05
798.90	-31.89	325.58
703.35	-25.56	321.62
616.68	-18.37	320.01
537.26	-13.67	316.26
464.04	-8.30	314.13
395.90	-5.07	310.17
332.74	-3.64	304.78
274.02	-3.33	291.22
168.93	-6.26	284.45
121.51	-5.91	279.93
76.52	-3.28	278.11
33.46	-0.18	276.99
-7.81	2.50	275.65
time = 18 Z		
Height (dm)	Temperature (c)	Potential Temperature (K)
893.64	-40.43	328.17
787.60	-34.67	321.82
692.72	-26.64	320.21
606.74	-21.16	316.52
528.17	-15.94	313.50
455.60	-10.64	311.36
388.04	-6.47	308.55
325.10	-4.51	303.79
266.64	-4.66	297.26
212.44	-6.04	289.97
162.03	-7.18	283.46
114.72	-6.16	279.67
69.73	-3.14	278.25
26.65	-3.51	277.14
-14.65	2.64	275.79

time = 21 Z		
Height (dm)	Temperature (c)	Potential Temperature (K)
882.53	-40.19	328.52
776.51	-35.22	321.08
682.19	-28.57	317.71
596.79	-22.57	314.74
518.59	-17.07	312.11
446.43	-12.47	309.19
379.39	-8.29	306.44
316.90	-6.43	301.62
258.92	-7.00	294.68
205.25	-8.64	287.15
155.31	-9.30	281.20
108.29	-7.24	278.54
63.45	-3.70	277.68
20.49	-0.82	276.35
-20.67	1.85	275.00

time = 24 Z		
Height (dm)	Temperature (c)	Potential Temperature (K)
872.48	-40.30	328.36
767.17	-37.09	318.56
673.37	-29.86	316.03
588.64	-24.95	311.75
511.07	-18.74	310.08
439.43	-14.66	306.60
373.22	-12.82	301.21
312.09	-12.63	294.61
255.57	-13.40	287.60
203.15	-13.96	281.38
154.08	-12.77	277.51
107.58	-9.82	275.83
63.18	-6.11	275.19
20.61	-3.24	273.90
-20.17	-0.59	272.56

time = 27 Z		
Height (dm)	Temperature (c)	Potential Temperature (K)
867.92	-42.25	325.61
763.39	-38.51	316.64
669.95	-30.38	315.35
585.43	-25.76	310.73
508.24	-20.32	308.15
437.37	-18.75	301.75
372.39	-17.65	295.61
312.40	-17.33	289.30
256.88	-17.55	283.00
205.25	-17.65	277.37
156.89	-16.37	273.67
111.01	-12.98	272.52
67.13	-9.20	272.01
25.05	-6.16	270.93
-15.29	-3.54	269.61
time = 30 Z		
Height (dm)	Temperature (c)	Potential Temperature (K)
865.70	-43.41	323.97
761.62	-39.64	315.12
668.59	-31.27	314.20
584.42	-26.95	309.23
507.92	-23.54	304.23
438.11	-23.12	296.57
374.32	-22.07	290.51
315.31	-21.10	285.03
260.58	-21.02	279.16
209.64	-20.56	274.21
161.67	-17.90	272.04
116.03	-14.19	271.25
72.35	-10.46	270.71
30.45	-7.27	269.81
-9.72	-4.66	268.49

time = 33 Z		
Height (dm)	Temperature (c)	Potential Temperature (K)
863.65	-43.74	323.50
760.07	-41.42	312.71
667.75	-32.99	311.97
584.30	-29.36	306.20
508.60	-26.26	300.91
439.59	-26.22	292.89
376.65	-25.18	286.91
318.29	-23.50	282.32
264.03	-22.72	277.28
213.35	-21.77	272.90
165.66	-19.59	270.24
120.32	-15.94	269.42
76.93	-12.09	269.03
35.27	-8.62	268.44
-4.69	-6.02	267.13

time = 36 Z		
Height (dm)	Temperature (c)	Potential Temperature (K)
861.93	-43.27	324.17
758.87	-43.81	309.48
667.50	-35.29	308.97
584.96	-32.33	302.47
510.05	-28.07	298.71
441.38	-27.10	291.83
378.69	-26.57	285.29
320.74	-25.30	280.28
266.84	-24.38	275.43
216.55	-23.95	270.53
169.27	-21.75	267.93
124.31	-18.02	267.24
81.27	-14.09	266.97
39.90	-10.37	266.66
0.22	-7.79	265.36

time = 39 Z		
Height (dm)	Temperature (c)	Potential Temperature (K)
861.60	-42.00	325.96
757.89	-43.26	310.23
667.07	-38.38	304.96
585.33	-33.76	300.68
510.95	-30.43	295.83
442.96	-29.19	289.37
380.76	-28.46	283.11
323.27	-27.07	278.28
269.68	-25.37	274.35
219.61	-25.14	269.23
172.60	-23.54	266.02
127.92	-19.34	265.86
85.08	-15.15	265.87
43.83	-10.81	266.21
4.21	-8.23	264.92

Appendix B

List of Symbols

C_n	Structure parameter of the refractive index fluctuation
D	Melted diameter of snowflake
Δf	Doppler Shift
ε	Energy dissipation rate
f	Frequency of the radar
K	Constant
L_B	Outer scale of turbulence (or Buoyancy scale)
λ	Wavelength of the profiler
$N(D)$	Snowflake size distribution
N	Brunt-Väisälä frequency
R	Rainrate
Ri	Richardson Number
$s(v)$	Power spectrum of Velocity
S_t	Total wind shear
S_s	Speed wind shear
S_d	Directional wind shear

$\mathbf{r}$	vectorial radial distance
σ_s^2	Spectral variance
σ_t^2	Variance due to turbulence
σ_f^2	Variance due to fall speed distribution
σ_w^2	Variance due to cross-beam wind
σ_r^2	Residual variance
σ_{Tot}^2	Total variance due to turbulence
$\sigma_{<v>}^2$	Variance of mean vertical velocity
θ	Beamwidth of the profiler
v_s	Fall speed of snowflakes
v_r	Radial vertical velocity as seen by the radar
V	Horizontal wind speed
$\mathbf{V}$	Vectorial target velocity (in chapter 1)
	Horizontal wind speed vector (in chapters 3 and 4)
w	Vertical wind
Z	Reflectivity

References

[1] D. Atlas and R.C. Srivastava. "A Method for Radar Turbulence Detection". *IEEE Transactions on Aerospace and Electronic Systems*, 7(1):179–187, 1970.

[2] A. R. Bohne. "Radar Detection of Turbulence in Precipitation Environments". *Journal of Atmospheric Sciences*, 39(August):1819–1837, 1982.

[3] J.A. Børresen. "Doppler Radar Study of Shear Zones and Turbulence in a Snowstorm". *Journal of Applied Meteorology*, 10:433–442, june 1971.

[4] W.Y. Chen. "Energy Dissipation Rates of Free Atmosheric Turbulence". *Journal of the Atmospheric Sciences*, 31:2222–2225, 1974.

[5] C.O.Hines. "Generalization of the Richardson Criterion for the Onset of Atmospheric Turbulence". *Quartely Journal Royal Meteorology Society*, 97:429–439, 1971.

[6] S. A. Cohn. *Investigation Of Atmospheric Turbulence With Radar and Thermodynamic Soundings.* PhD thesis, Massachusetts Institude of Technology, 1991.

[7] A.S. Frisch and S.F. Clifford. "A Study of Convection Capped by a Stable Layer Using Doppler Radar and Acoutic Echo Sounder". *Journal of the Atmospheric Sciences*, 31:1622–1628, 1974.

[8] E.E. Gossard. " Radar Research on the Atmospheric Boundary Layer". *Radar in Meteorology*, Edited by D.Atlas, AMS, Boston:477–527, 1990.

[9] E.E. Gossard, R.B Chadwick, T.R. Detman, and J. Gaynor. "Capability of Surface-Based Clear-Air Doppler Radar for Monitoring Meteorological Structure of Elevated Layers". *Journal of Climate and Applied Meteorology*, 23:474–1405, 1984.

[10] K.L.S. Gunn and J.S. Marshall. " The Distribution with Size of Aggregate Snowflakes". *Journal of Meteorology*, 6:452–461, 1949.

[11] K.R. Hardy and K.S. Gage. " The History of Radar Studies of the Clear Atmosphere". *Radar in Meteorology*, Edited by D.Atlas, AMS, Boston:130–142, 1990.

[12] W. Hitschfeld and A.S. Dennis. "Measurement and Calculation of Fluctuations in Radar Echoes from Snow". *Scientific report No. MW-23,McGill Univ.*, 1956.

[13] W.K. Hocking. "Mesospheric Turbulence Intensities Measured with a HF Radar at 35° - II". *Journal of Atmospheric and Terrestrial Physics*, 45(2/3):103–114, 1983.

[14] W.K. Hocking. "Measurement of Turbulence Energy Dissipation Rates in the Middle Atmosphere by Radar Techniques: A review". *Radio Science*, 20(6):1403–1422, 1985.

[15] W.K. Hocking. "Observation and Measurement of Turbulence in the Middle Atmosphere with a VHF Radar". *Journal of Atmospheric and terrestrial Physics*, 48(7):665–670, 1986.

[16] Z. Huo, D.-L. Zhang, J. Gyakum, and A. Staniforth. " A Diagnostic Analysis of the Superstorm of March 1993". *Monthly Weather Review*, To appear.

[17] M.P. Langleben. "The Terminal Velocity of Snowflakes". *Quart. J. Roy. Meteor. Soc.*, 80:174–181, 1954.

[18] R. R. Rogers, W. L. Ecklund, D.A. Carter, K. S. Gage, and S.A. Ethier. "Research Application of a Boundary-Layer Wind Profiler". *Buletin of the American Meteorological Society*, 74(4):567–80, 1993.

[19] R.R. Rogers and B.R. Tripp. "Some Radar Mesurement of Turbulence in Snow". *Journal of Applied Meteorology*, 3(5):603–610, 1964.

[20] R.R. Rogers and M.K. Yau. *A Short Course in Cloud Physics.* Pergamon Press, 1989.

[21] Kaoru Sato. "Vertical Wind Disturbances in the Troposphere and Lower Stratosphere Observed by the MU Radar". *Journal of the Atmospheric Sciences*, 47(23):2803–2817, 1990.

[22] H. Sauvageot. *"Radar Meteorology".* Artech House, Norwood, 1992.

[23] T.E. VanZandt, S.A. Smith, T.Tsuda, T.Sato, S.Fukao, and S. Kato. "Studies of Velocity Fluctuation in the Lower Atmosphere Using the Mu Radar. Part I: Azimuthal Anisotropy". *Journal of the Atmospheric Sciences*, 47(1):39–47, 1990.

[24] A. Vincent and M. Meneguzzi. "The Spatial Structure and Statistical Properties of Homogeneous Turbulence". *Journal of Fluid Mechanics*, 225:1–20, 1991.

[25] V.I.Tatarskii. *Wave Propagation in a Turbulent Medium.* McGraw Hill, New York, 1961.

[26] J. Weinstock. "Vertical Turbulent Diffusion in a Stably Stratified Fluid". *Journal of Atmospheric Sciences*, 35:1022–1027, June 1978.